Check for updates

AGU ADVANCING EARTH AND SPACE SCIENCES

Earth's Future

RESEARCH ARTICLE
10.1029/2025EF007458

Key Points:

- High-resolution modeling is crucial for accurately estimating the heterogeneous urban biogenic and anthropogenic CO_2 fluxes
- Urban vegetation offers significant carbon-buffering potential. In Munich, trees are primary CO_2 sinks, grasslands are net sources
- The model's promising performance was validated by our urban biogenic measurements, showing that our model is applicable in urban scenarios

Supporting Information:

Supporting Information may be found in the online version of this article.

Correspondence to:

J. Li and J. Chen,
junwei.li@tum.de;
jia.chen@tum.de

Citation:

Li, J., Chen, J., Glauch, T., Brunner, D., Marshall, J., Ponomarev, N., et al. (2026). Fine-scale estimation of urban biogenic CO_2 fluxes: A novel framework integrating multiple versions of vegetation photosynthesis and respiration models and in situ measurements. *Earth's Future*, *14*, e2025EF007458. https://doi.org/10.1029/2025EF007458

Received 30 SEP 2025
Accepted 3 FEB 2026

© 2026. The Author(s).
This is an open access article under the terms of the Creative Commons Attribution License, which permits use, distribution and reproduction in any medium, provided the original work is properly cited.

Fine-Scale Estimation of Urban Biogenic CO_2 Fluxes: A Novel Framework Integrating Multiple Versions of Vegetation Photosynthesis and Respiration Models and In Situ Measurements

Junwei Li[1], Jia Chen[1], Theo Glauch[2,3], Dominik Brunner[4], Julia Marshall[2], Nikolai Ponomarev[4], Haoyue Tang[1], and Stavros Stagakis[5]

[1]Environmental Sensing and Modelling, School of Computation, Information and Technology, Technical University of Munich, Munich, Germany, [2]Institute of Atmospheric Physics, German Aerospace Center (DLR), Oberpfaffenhofen, Germany, [3]Institute of Environmental Physics, Heidelberg University, Heidelberg, Germany, [4]Laboratory for Air Pollution/Environmental Technology, Swiss Federal Laboratories for Materials Science and Technology, Empa, Dübendorf, Switzerland, [5]Department of Environmental Sciences, University of Basel, Basel, Switzerland

Abstract Estimating biogenic CO_2 fluxes is essential to quantify urban anthropogenic emissions, yet urban vegetation heterogeneity presents a significant challenge to making accurate estimations. We have developed an hourly temporal, 10-m spatial resolution biogenic CO_2 flux estimation framework based on the Vegetation Photosynthesis and Respiration Model (VPRM) and its variants (UrbanVPRM and VPRM-modified). Unlike lower-resolution models, our approach captures finer-scale variability, particularly in fragmented urban green spaces like street trees and lawns. Results show that vegetation in Munich offsets 2.0%–2.8% of annual anthropogenic CO_2 emissions in the study domain, with tree-covered areas as primary sinks and grasslands as net sources. During summer, daytime CO_2 uptake can match or exceed anthropogenic emissions. Evaluations employing city park field measurements and eddy covariance towers confirm strong performance of our models, while highlighting VPRM-modified's advantage in grasslands and croplands, and UrbanVPRM's improvements in urban areas via impervious surface correction. These findings highlight the value of high-resolution modeling in improving urban carbon flux assessments.

Plain Language Summary Cities are emitters of carbon dioxide (CO_2) from human activities like traffic and heating, but green spaces like lawns and street trees also absorb and release CO_2. To accurately calculate how much CO_2 humans are truly responsible for, we need to precisely estimate the CO_2 exchange from the city's complex and varied vegetation. To solve this, we developed a framework to map this vegetation CO_2 exchange in Munich and Zurich, creating hour-by-hour estimates at a fine 10-m resolution, which can resolve the impact of small green patches, like individual street trees and lawns. This high-resolution approach is further validated against our field measurements from city parks and tower measurements from rural areas. Results show that Munich's vegetation offsets about 2.0%–2.8% of its annual human-caused CO_2 emissions. Tree-covered areas are the primary sinks that absorb CO_2, while grasslands tend to be minor sources that release it. Remarkably, the greenery's CO_2 absorption on a summer day can temporarily outweigh Munich's entire human emissions. This transferable framework enables an accurate evaluation of the carbon sequestration benefits of urban green infrastructure, ultimately providing policymakers with precise data to support more effective climate strategies and urban planning policies.

1. Introduction

As the main driver of global warming, the growth rate of anthropogenic carbon dioxide (CO_2) emissions has become a pressing global issue (Meyer et al., 2014). Although only a fraction of fossil fuel CO_2 emissions physically occur within city boundaries, urban areas are estimated to account for up to 70% of global CO_2 emissions when indirect emissions from energy use and supply chains are considered (Seto et al., 2014; Turnbull et al., 2019; Velasco & Roth, 2010). As a result, numerous countries and cities have committed to reducing urban CO_2 emissions, with many aiming to achieve net-zero carbon emissions by 2050 or earlier. To support these efforts, all CO_2 sources and sinks must be identified and emission inventories validated (Bezyk et al., 2021; Wei et al., 2022). While urban vegetation plays an important role in net CO_2 emissions, impacting both spatial and

23284277, 2026, 3, Downloaded from https://agupubs.onlinelibrary.wiley.com/doi/10.1029/2025EF007458 by Dtsch Zentrum F. Luft-U. Raum Fahrt In D. Helmholtz Gemein., Wiley Online Library on [09/09/2026]. See the Terms and Conditions (https://onlinelibrary.wiley.com/terms-and-conditions) on Wiley Online Library for rules of use; OA articles are governed by the applicable Creative Commons License

temporal variability in atmospheric CO_2 concentrations, accurate assessment of CO_2 fluxes from urban vegetation remains challenging (Stagakis, Feigenwinter, Vogt, & Kalberer, 2023; Velasco & Roth, 2010; Wei et al., 2022; Weissert et al., 2014; Wu et al., 2021). Quantifying these biogenic CO_2 fluxes is particularly critical for understanding the anthropogenic CO_2 emissions in cities, especially when integrated into atmospheric transport models and validated against observed concentrations.

The biogenic CO_2 flux refers to the amount of CO_2 released to or absorbed from the atmosphere by biological activities within an ecosystem, including CO_2 uptake via photosynthesis and its release through respiration by vegetation and soil microorganisms (Schimel, 1995). In recent years, many models have been developed to estimate the urban vegetation CO_2 flux (Sargent et al., 2018; Stagakis, Brunner, et al., 2025). For example, the Surface Urban Energy and Water Balance Scheme (SUEWS) (Järvi et al., 2011; Leena Järvi et al., 2019) uses meteorological, urban structures, and land cover to simulate urban energy, carbon, and water cycles at the local scale. Jena Scheme for Biosphere-Atmosphere Coupling in Hamburg (JSBACH) (Reick et al., 2013), the land component of the Max Planck Institute Earth system model (MPI-ESM) (Giorgetta et al., 2013), was applied by Thölix et al. (2025) to simulate the full land carbon cycle, including photosynthetic and respiratory processes as well as changes in carbon pools in diverse types of urban vegetation. The diFUME model employs a semi-empirical approach, using meteorological information along with high-resolution urban vegetation morphologies and the leaf area index (LAI), to estimate urban biogenic CO_2 fluxes (Stagakis, Feigenwinter, Vogt, & Kalberer, 2023). These models are capable of estimating the annual, seasonal, and even diurnal biogenic carbon fluxes, yet their applicability in urban settings is limited by the difficulty of deployment and the availability and resolution of required input data.

Eddy covariance (EC) flux towers provide direct, high-frequency measurements of the CO_2 exchange between the land surface and the atmosphere, and have been widely used to monitor the Net Ecosystem Exchange across various ecosystems (Baldocchi et al., 2001; Rosentreter, 2022) and more recently in cities (Leena Järvi et al., 2018). Although EC towers built inside cities measure the total CO_2 flux, including anthropogenic and biological emissions, researchers have attempted to isolate the biogenic component. Menzer and McFadden (Menzer & McFadden, 2017) created an inventory of anthropogenic emissions, and subtracted these emissions from the EC tower measurement of the CO_2 flux. Wu et al. (2022) used atmospheric measurements of CO_2 and CO mole fractions combined with a ^{14}C isotope analysis to estimate fossil fuel emissions and thereby derive the biological CO_2 flux. Stagakis, Feigenwinter, Vogt, Brunner, et al. (2023) employed a Bayesian framework to assimilate EC observations and to partition fluxes into source and sink components using a footprint model. Despite these advances, the biogenic CO_2 fluxes derived from EC measurements remain uncertain and spatially limited to the tower's footprint, making it difficult to obtain high-resolution maps of biogenic CO_2 fluxes for entire cities.

In contrast to comprehensive but relatively complex biogenic models and inherently constrained EC measurements, the Vegetation Photosynthesis and Respiration Model (VPRM) (Mahadevan et al., 2008a) stands out as a lightweight, satellite-based, and data-driven model while achieving exceptional performance. VPRM partitions the Net Ecosystem Exchange (NEE) into a light-dependent part, the Gross Ecosystem Exchange (GEE), and a light-independent part, ecosystem respiration. To drive the model, VPRM utilizes the Enhanced Vegetation Index (EVI) and the Land Surface Water Index (LSWI) computed from reflection measured by satellite instruments, such as the Moderate Resolution Imaging Spectroradiometer (MODIS), along with air temperature and Photosynthetically Active Radiation (PAR). VPRM requires only a few parameters, which are estimated from flux tower measurements over the respective ecosystems, to describe photosynthesis and respiration of a given type of vegetation. Due to its simplicity and good performance, VPRM has been widely incorporated into atmospheric transport models such as WRF-Chem and ICON-ART (Ahmadov et al., 2009; Ponomarev et al., 2023; Zhao et al., 2023). However, the model's simple formulation and coarse-resolution input data, originally intended for rural landscapes, limit its accuracy in urban settings. To improve VPRM's usefulness in cities, several modified versions have been proposed. The UrbanVPRM (Hardiman et al., 2017a) improved the respiration component by distinguishing between heterotrophic and autotrophic respiration and incorporating the Impervious Surface Area (ISA) through an EVI-ISA correction. The VPRM-modified version by Gourdji et al. (2022) introduced a nonlinear temperature-respiration relationship and incorporated additional vegetation indices, increasing the accuracy of the model at the expense of higher complexity.

However, most VPRM applications still rely on MODIS-based vegetation indices at 500-m resolution, which is inadequate for capturing the biogenic CO_2 flux in densely built urban environments. Recent studies have attempted to use vegetation indices from higher-resolution Landsat and Sentinel-2 satellites. Winbourne et al. (2022) used Landsat to drive UrbanVPRM in fragmented urban temperature forests and unmanaged grasslands, validating their results with in situ observations. Wei et al. (2022) employed Landsat and UrbanVPRM to estimate vegetation NEE at 30-m resolution in New York, but focused only on trees and grasslands within the study area. However, these studies still do not provide a comprehensive assessment of the NEE of all urban and peri-urban vegetation, nor do they thoroughly compare the results of these various VPRM implementations or evaluate their performance in urban settings.

This study focuses on estimating biogenic CO_2 fluxes in Munich and Zurich at tree-resolving scale with improved accuracy, by evaluating the performance of different variants of the VPRM model using comprehensive vegetation flux observations in the two cities. The main contributions of this article are as follows: We developed a 10-m spatial, hourly temporal resolution estimation framework for biogenic CO_2 fluxes in Munich and Zurich using three variants of the VPRM model: the standard VPRM, UrbanVPRM, and VPRM-modified. The framework was designed to be scalable and transferable to other cities. Furthermore, we explored the advantages of the high-resolution VPRM model by systematically comparing it with a coarse-resolution VPRM product. By integrating data from ecosystem observation stations across Europe, we calibrated and comprehensively evaluated the performance of all three VPRM variants. Furthermore, using data collected from our urban measurement campaigns in Munich and Zurich city parks, we assessed the performance of the different VPRM versions within urban environments. Based on these results, we analyzed the differences among the VPRM versions to provide deeper insights into urban vegetation CO_2 fluxes and uncertainties in their results. Although the framework is applied to both cities, the analysis focuses on the results from Munich. Our framework should help reduce the uncertainties in quantifying urban anthropogenic CO_2 emissions and potentially support the formulation of effective CO_2 emission reduction policies for cities.

2. Methods

2.1. Study Areas

Our research targeted the urban regions of Munich and Zurich, which are two of the three pilot cities of the ICOS-Cities PAUL (Pilot Application in Urban Landscapes) project. In Munich, the study domain spans approximately 84 km × 84 km (7,056 km^2), as depicted in Figure 1, but mainly focus on a smaller area of about 23 km × 29 km (667 km^2). The larger domain allows for a comparison of our VPRM results with other existing VPRM products, while the smaller domain is more representative of urban biogenic CO_2 fluxes. The Zurich study domain encompasses about 13 km × 14 km (182 km^2), as indicated in Figure 2.

2.2. High Resolution VPRM Framework

In this section, we present our high-resolution biogenic CO_2 estimation framework based on the standard VPRM, UrbanVPRM, and VPRM-modified model, along with a comprehensive description of the required data sets and the procedures used for their construction and processing. The description of VPRM models are detailed in Supporting Information S1. Briefly, the standard VPRM calculates NEE by partitioning it into GEE and respiration based on satellite-derived vegetation indices (EVI/LSWI) and meteorological data (temperature/PAR). UrbanVPRM refines this for urban areas by splitting respiration into autotrophic and heterotrophic components and incorporating ISA, while VPRM-modified introduces a nonlinear temperature relationship and additional vegetation indices to the respiration formula. The outputs from the different variants of VPRM for all study areas are at a spatial resolution of 10 m and a temporal resolution of 1 hour.

2.2.1. Vegetation Indices

All three VPRM models require the vegetation indices EVI and LSWI as input, which serve as the observation of vegetation phenology and water stress. To derive biospheric fluxes at 10 m resolution, we here derive the EVI and LSWI indices from high-resolution observations from the Sentinel-2 multispectral imaging satellite. Compared to the MODIS satellite used in most previous studies, Sentinel-2 offers a much higher resolution of up to 10 m.

23284277, 2026, 3, Downloaded from https://agupubs.onlinelibrary.wiley.com/doi/10.1029/2025EF007458 by Dtsch Zentrum F. Luft-U. Raum Fahrt In D. Helmholtz Gemein., Wiley Online Library on [09/09/2026]. See the Terms and Conditions (https://onlinelibrary.wiley.com/terms-and-conditions) on Wiley Online Library for rules of use; OA articles are governed by the applicable Creative Commons License

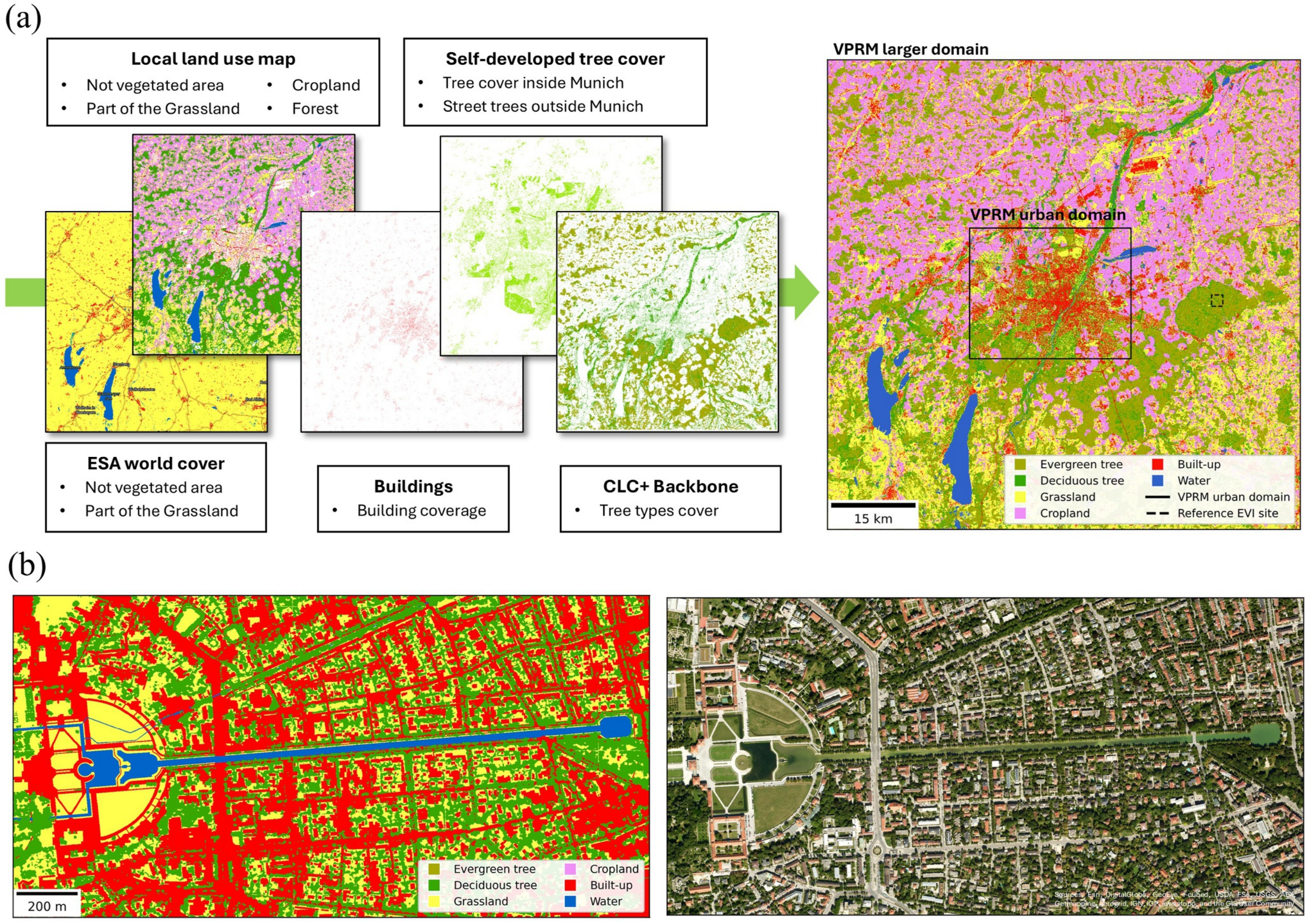

Figure 1. Self-developed vegetation land cover map for Munich. (a) Process flow for generating the vegetation land cover map. This map represents the largest VPRM domain for Munich in the study. The black boundary delineates the VPRM urban domain, while the dashed boundary indicates the reference EVI region used for UrbanVPRM. (b) Comparison of the self-developed 1 m resolution vegetation land cover map with a satellite image at Munich Schloss Nymphenburg. Satellite image source: Esri, DigitalGlobe, GeoEye, i-cubed, USDA FSA, USGS, AEX, Getmapping, Aerogrid, IGN, IGP, swisstopo, and the GIS User Community (Esri, 2025).

We employed the "Sentinel-2 MSI—Level 2A (MAJA Tiles)—Germany" data set produced by the German Aerospace Center (DLR) (German Aerospace Center, 2019), which covers our study areas in both Munich and Zurich. This data set includes an atmospheric correction of the original Sentinel-2 observations and provides mask layers for clouds, cloud shadows, and snow. Masked pixels are treated as invalid.

Sentinel-2 has 13 spectral channels. To calculate EVI and LSWI, only bands 2, 4, 8, and 11 are used, corresponding to blue, red, near-infrared (NIR), and short-wave infrared (SWIR), respectively. While the blue, red, and NIR bands have a 10-m spatial resolution, the SWIR band has only 20-m resolution. To retain the high-resolution information of other bands, the SWIR band was resampled to 10-m resolution by subdividing each 20-m pixel into four equal 10-m pixels through regriding. The EVI and LSWI are calculated with the following formula (Mahadevan et al., 2008b):

$$\mathrm{EVI} = G \times \frac{\mathrm{NIR} - \mathrm{Red}}{\mathrm{NIR} + C_1 \times \mathrm{Red} - C_2 \times \mathrm{Blue} + L} \tag{1}$$

$$\mathrm{LSWI} = \frac{\mathrm{NIR} - \mathrm{SWIR}}{\mathrm{NIR} + \mathrm{SWIR}} \tag{2}$$

23284277, 2026, 3, Downloaded from https://agupubs.onlinelibrary.wiley.com/doi/10.1029/2025EF007458 by Dtsch Zentrum F. Luft-U. Raum Fahrt In D. Helmholtz Gemein., Wiley Online Library on [09/09/2026]. See the Terms and Conditions (https://onlinelibrary.wiley.com/terms-and-conditions) on Wiley Online Library for rules of use; OA articles are governed by the applicable Creative Commons License

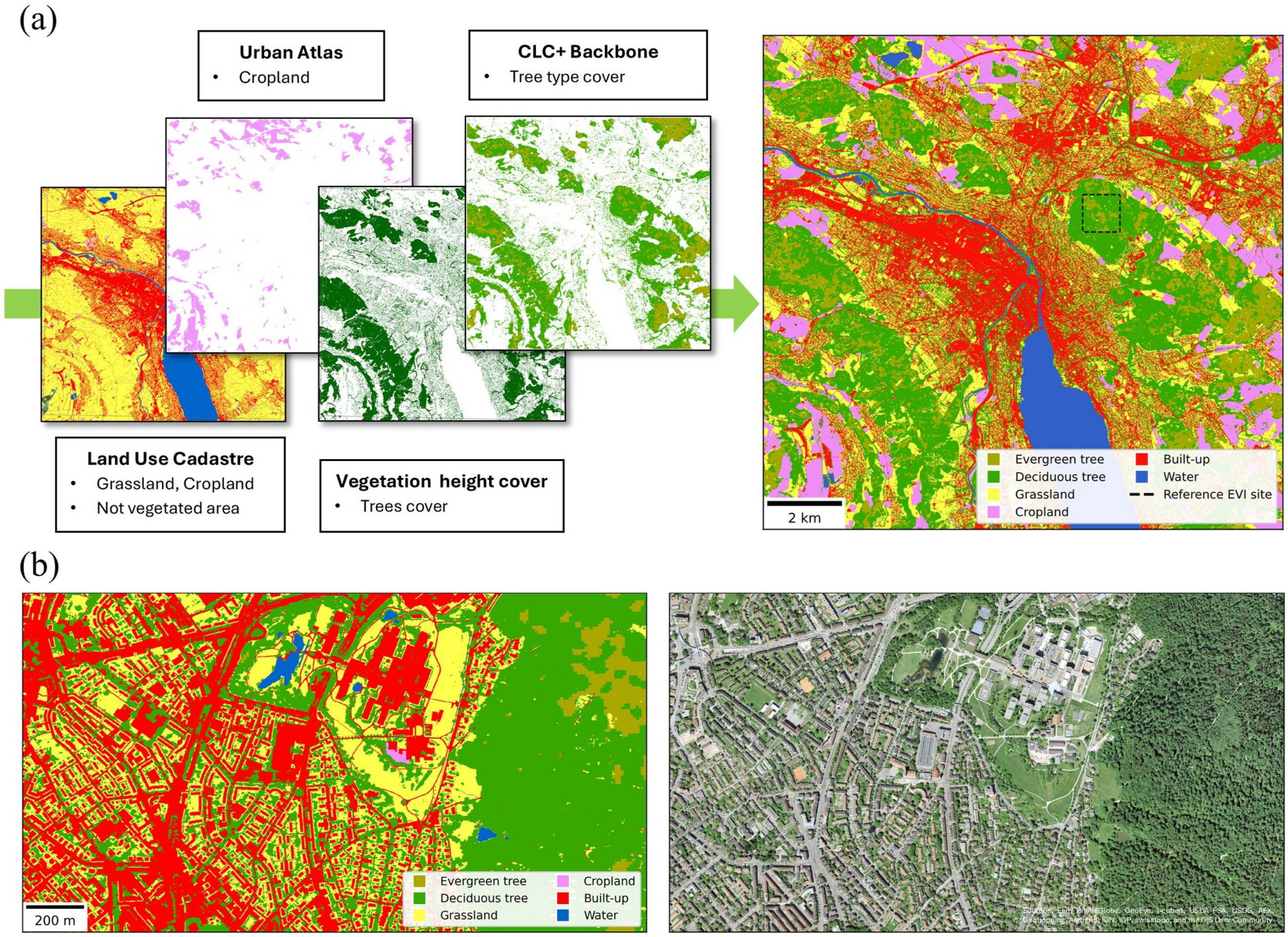

Figure 2. Self-developed vegetation land cover map for Zurich. (a) Process flow for generating the vegetation land cover map. This map represents the VPRM domain for Zurich in the study. The dashed boundary indicates the reference EVI region used for UrbanVPRM. (b) Comparison of the self-developed 1-m resolution vegetation land cover map with a satellite image near Zurich Irchelpark. Satellite image source: Esri, DigitalGlobe, GeoEye, i-cubed, USDA FSA, USGS, AEX, Getmapping, Aerogrid, IGN, IGP, swisstopo, and the GIS User Community (Esri, 2025).

where, $G = 2.5$, $C_1 = 6$, $C_2 = 7.5$ and $L = 1$ (Askar et al., 2018; Huete et al., 2002; Son et al., 2020). The calculated EVI values are then restricted to the valid range of 0–1, and LSWI from −1 to 1 to eliminate the effect of extreme values or noise.

The derived EVI and LSWI images were then linearly interpolated to daily resolution and smoothed using the locally weighted scatterplot smoothing (LOWESS, Cleveland, 1979) filter to reduce noise and smooth the time series for each pixel, with the span set to 0.3 and iterations set to 3.

2.2.2. Vegetation Land Cover Map

A vegetation land cover map is needed to assign the vegetation type for each satellite pixel. To fully utilize the high-resolution vegetation index information provided by Sentinel-2, a corresponding 10-m × 10-m resolution vegetation land cover map is required. The vegetation land cover maps for Munich and Zurich were created separately to make use of the highest quality data sets available in the two cities.

2.2.2.1. Munich

The Real Estate Cadastre Information System ALKIS from the Bavarian State Office for Digitization, High-Speed Internet and Surveying (LDBV) (Bayerische Vermessungsverwaltung, 2024) provides a detailed map of Munich with 140 different land use types. From this data set, we extracted the grassland, the cropland, the forest

23284277, 2026, 3, Downloaded from https://agupubs.onlinelibrary.wiley.com/doi/10.1029/2025EF007458 by Dtsch Zentrum F. Luft-U. Raum Fahrt In D. Helmholtz Gemein., Wiley Online Library on [09/09/2026]. See the Terms and Conditions (https://onlinelibrary.wiley.com/terms-and-conditions) on Wiley Online Library for rules of use; OA articles are governed by the applicable Creative Commons License

outside of Munich's administrative boundaries, and non-vegetated areas like buildings or water cover as a base map. The base map contained some gaps, which were filled using the 10-m resolution ESA World Cover map (Zanaga et al., 2022). To ensure compatibility with higher-resolution local data sets on tree cover and cropland—introduced below—and to preserve data on open glades within forested areas, the ESA World Cover map was modified by reclassifying tree and cropland areas as grassland. As a result, the final base map was primarily derived from local data sets, with the ESA World Cover data set serving only to fill gaps. The building coverage data set from LDBV is used to eliminate potential errors in the base map.

A tree canopy cover data set was generated using the laser point cloud data provided by LDBV and the Urban Atlas Street Tree Layer from the Copernicus Land Monitoring Service (European Environment Agency, 2020c). The laser point cloud data, measured by an aircraft to detect the terrain surface inside the Munich administrative boundaries, was processed using the LAStools software suite (LAStools, 2003) to derive the tree canopy cover. Tree canopies smaller than 10 m^2 or lower than 2 m were excluded to reduce noise. Outside Munich's administrative boundaries, the Urban Atlas Street Tree Layer was used for street tree cover, while the land cover map described before provided other tree cover, such as trees in forested areas. Finally, the CLC + Backbone data set (European Environment Agency, 2024) at 10 m × 10 m resolution was employed to classify the trees as deciduous or evergreen. Trees inside the city, where no information on tree type was available, were assumed to be deciduous.

All intermediate land cover maps were rasterized to 1-m resolution before merging into the final vegetation land cover map. The resulting maps were then resampled to the 10-m resolution grid of the Sentinel-2 data set using the majority resampling method (Esri, 2024). This process allows for maintaining the accuracy of the original information to the greatest extent without being affected by resampling. The overall workflow and the resulting vegetation land cover map are illustrated in Figure 1.

2.2.2.2. Zurich

The Land Use Cadastre of the Canton of Zurich from Zurich Kanton (Zürich Kanton, 2025) acted as our base map for the self-developed land cover map of Zurich. This data set provides a high-quality official land registry of the Canton. The original classifications of the data set were reclassified into grassland, cropland, and non-vegetated areas. The forests were reclassified to grassland and then overlaid by the more accurate local tree cover data, following the same idea as in Munich. Most cropland coverage in the Land Use Cadastre of the Canton of Zurich is mixed with grassland and cannot be separated. It was therefore reclassified as grassland, and the Urban Atlas 2018 (European Environment Agency, 2020b) from the Copernicus Land Monitoring Service was used instead to provide cropland coverage.

The tree coverage was determined from the Vegetation Height Model (VHM) from the Swiss federal forest inventory (https://www.lfi.ch/). This data set was created using stereo aerial images and LiDAR observations to produce a 1 m × 1 m resolution high-quality product. Trees lower than 2 m height were eliminated as these pixels were mostly noise. In the same way as for Munich, the CLC + Backbone was utilized to identify tree types. Trees not covered by the CLC + Backbone data set were classified as deciduous. The resulting tree cover map was then overlaid on the previously created base map to generate the final vegetation landcover map for Zurich. All intermediate maps were first rasterized to a 1-m resolution and merged, then resampled to 10-m resolution using a majority method—consistent with the Munich workflow. The complete process is illustrated in Figure 2.

The final vegetation land cover maps for both Munich and Zurich include only four types: deciduous, evergreen, grassland, cropland, and non-vegetated. The “Savanna” and “Mixed forest” classes from the original VPRM classes are not included as our land cover map can resolve different tree types as well as the trees within grassland fields, and the “shrubland” class is excluded since it did not exist within our study area.

2.2.2.3. Impervious Surface Area

The UrbanVPRM model requires additional Impervious Surface Area (ISA) ratios for each Sentinel-2 pixel. We utilized the Imperviousness Density 2018 data set (European Environment Agency, 2020a) from the Copernicus Land Monitoring Service. This data set is generated from Sentinel-1 and Sentinel-2 satellite data and provides the ISA fraction in the range from 0% to 100% at 10-m spatial resolution.

23284277, 2026, 3, Downloaded from https://agupubs.onlinelibrary.wiley.com/doi/10.1029/2025EF007458 by Dtsch Zentrum F. Luft-U. Raum Fahrt In D. Helmholtz Gemein., Wiley Online Library on [09/03/2026]. See the Terms and Conditions (https://onlinelibrary.wiley.com/terms-and-conditions) on Wiley Online Library for rules of use; OA articles are governed by the applicable Creative Commons License

2.2.3. Meteorological Fields and Observation

Air temperature at 2 m and downward solar radiation at the surface are the main drivers of the spatial-temporal behavior of VPRM. In order to represent temperature variations due to the urban heat island effect and topography, meteorological simulation results from the Weather Research and Forecasting model (WRF) and the Icosahedral Nonhydrostatic weather and climate model with Aerosols and Reactive Trace gases (ICON-ART) were used for Munich and Zurich, respectively.

For Munich, the WRF model Version 3.9.1.1 was deployed. The ERA5 hourly data on single levels (Hersbach et al., 2020) provided the meteorological initial and boundary conditions for the model, resulting in a final output with 400 m horizontal resolution covering the whole study area in Munich. Hourly temperature at 2 m (T2) and shortwave downward radiation (SWDOWN) were extracted from the WRF output for VPRM. For more details on our WRF setup in Munich, please refer to Zhao et al. (2023).

For Zurich, simulations were performed using ICON-ART for two nested domains, central Europe (6.5-km spatial resolution) and a domain surrounding the city of Zurich (0.5-km spatial resolution). The land use data was based on the CORINE Land Cover 2018 (European Environment Agency, 2019) for Europe, and our self-developed land cover described in Section 2.2.2 for Zurich. ERA-5 global reanalysis data (Hersbach et al., 2020) provided meteorological boundary and initial conditions for European simulations using a similar model configuration as described in Steiner et al. (2024). Furthermore, the European simulation was weakly nudged toward ERA-5 fields to keep the meteorology close to the analyzed meteorology. The output of the European simulation was then used as initial and boundary conditions for the high-resolution Zurich simulations, which were run freely without further nudging to ERA-5.

The model-simulated meteorological fields were used for the city-wide VPRM simulations. For the comparison with biogenic measurements in the city parks of Munich and Zurich, however, VPRM was driven by meteorological measurements in the close vicinity of the parks. In Munich, these measurements were sourced from the Stadtstation of the Meteorological Institute Munich (48.1478°N, 11.5734°E). In Zurich, they were obtained from the Hardau meteorological station (47.3813°N, 8.5099°E), which was installed in the framework of the ICOS Cities project (Figure S1 in Supporting Information S1).

As shown in Figure S2 of Supporting Information S1 and as demonstrated by previous studies (Chen et al., 2014; Li et al., 2019; Yang et al., 2012), both WRF and ICON-ART can effectively reproduce urban-rural temperature differences. Comparison with ground observations in Table S1 of Supporting Information S1 demonstrates good agreement between simulated temperatures and shortwave downward radiation with observations.

2.2.4. Parameters for Different VPRM Versions

The parameters for the VPRM as well as the respiration parameters for the VPRM-modified model, were fitted using a methodology similar to that described in Glauch et al. (2025), using eddy covariance towers across Europe. The parameters for UrbanVPRM were the same as those in the VPRM following the recommendations of the original UrbanVPRM paper (Hardiman et al., 2017a). The GEE parameters of the VPRM-modified were also the same as those of the VPRM, but the respiration parameters were fitted individually.

Eddy covariance data were sourced from the ICOS ecosystem stations network final quality (L2) product (ICOS RI et al., 2024), which provides CO_2 NEE measurements as well as temperature and solar radiation. Due to the varying data availability across sites, for each vegetation type, 730 days (equivalent to 2 years) were randomly sampled from the period between 2015 and 2023, and data from these days were extracted. The complete list of selected flux towers is in Table S2 of Supporting Information S1.

Vegetation indices around each eddy covariance tower were extracted from Sentinel-2 Collection-1 Level-2A (L2A) data set (European Space Agency, 2022), which provides global coverage, accessed via the "*Terrabyte*" platform (German Aerospace Center, 2025). To ensure high data quality, we applied the same filtering and interpolation approach as described in Section 2.2.1. For each site, vegetation indices were extracted from the pixel corresponding to the tower location and neighbouring pixels (a 3×3 window covering 30 m $\times$ 30 m), and then averaged to represent the vegetation index at that site.

Respiration parameters for all VPRM models were first estimated using nighttime NEE observations, assumed to reflect respiration-only conditions. These fitted parameters were subsequently applied to predict respiration over

23284277, 2026, 3, Downloaded from https://agupubs.onlinelibrary.wiley.com/doi/10.1029/2025EF007458 by Dtsch Zentrum F. Luft-U. Raum Fahrt In D. Helmholtz Gemein., Wiley Online Library on [09/03/2026]. See the Terms and Conditions (https://onlinelibrary.wiley.com/terms-and-conditions) on Wiley Online Library for rules of use; OA articles are governed by the applicable Creative Commons License

10.1029/2025EF007458

the entire time period and combined with all-day NEE observation data to estimate GEE parameters. The temperature-related parameters T_{min}, T_{max}, T_{opt} and T_{low} were taken from Glauch et al. (2025), while all the other parameters were optimized via nonlinear least squares regression. The optimization was repeated 10 times to reduce the impact of stochastic variability in the fitting, and the parameter set yielding the lowest mean squared error (MSE) was selected. The complete set of parameters is presented in Table S3 of Supporting Information S1.

The VPRM models were implemented using Python 3.8.1 and simulated on the supercomputer provided by the German Climate Computing Center (Deutsches Klimarechenzentrum, DKRZ), with each computation node containing 128 physical CPU cores. The simulation time for 1 year in each model costs around 2,800 core hr for the larger Munich domain and around 80 core hr for the Zurich domain.

2.3. Comparison of Simulated CO_2 Fluxes With ICOS-VPRM Product and With Observations

2.3.1. ICOS-VPRM

We compared our VPRM results in Munich with the "Biosphere-atmosphere exchange fluxes for CO_2 from the Vegetation Photosynthesis and Respiration Model VPRM for 2006–2022 product" provided by the ICOS Data Portal (ICOS-VPRM) (Gerbig & Koch, 2023). ICOS-VPRM, employing an offline implementation of the standard VPRM model, incorporates MODIS-derived vegetation indices, 2-m temperature and shortwave downward radiation at the surface from ECWMF IFS analysis data, along with the 1-km resolution synergetic land cover data set (SYNMAP) (Jung et al., 2006), to provide hourly NEE, GEE, and ecosystem respiration outputs at ∼0.1-degree spatial resolution (approximately 11 km north–south and 7 km east–west in Munich).

To compare our VPRM results with the ICOS-VPRM results, we extracted 62 ICOS-VPRM pixels located entirely within our Munich study domain (larger domain in Figure 1), and upscaled our results from standard VPRM model (self-developed VPRM-std) to the same spatial resolution.

2.3.2. Eddy Covariance (EC) Towers

To evaluate the performance of the three VPRMs against observations, we utilized eddy covariance towers across Europe that measured vegetation CO_2 flux within ecosystems. Although the observational data were previously used to fit the parameters of the VPRM models, they remain valuable for assessing the different models under identical conditions. The measurements of CO_2 fluxes, temperature, and solar radiation, along with the vegetation indices derived from Sentinel-2 used to drive the VPRM models, were the same as those described in Section 2.2.4. From each site, we selected the 2 years with the best temporal coverage. The full list of selected EC towers and years is shown in Table S2 of Supporting Information S1.

As only the net CO_2 flux (NEE) is observed directly, to compare the GEE and respiration results, we used the Gross Primary Production (GPP, equal to -1*GEE) and respiration values extracted from observed NEE using the nighttime partitioning method provided by each EC tower. Although the partitioning method introduces some uncertainty, these results are sufficient for comparing the behavior of the three VPRM models.

2.3.3. Biogenic CO_2 Fluxes in Urban Parks

To validate the VPRM models results inside urban areas, we also need to validate them against urban measurements. In the framework of the ICOS-Cities project, urban ecophysiological field measurements were conducted in selected parks in Munich during 2024 and Zurich during 2023, as shown in Figure 3. The field measurements included tree sap flow, soil temperature (T_{soil}), soil water content (ϑ), as well as regular field campaigns to measure leaf area index (LAI) of selected trees using a ceptometer instrument and gas exchange of soils and grass leaves using flux chambers. The field measurements are described in detail in Stagakis, Brunner, et al. (2025) and can be found open access in the ICOS-Cities repository (Lan et al., 2025; J. Li et al., 2025a, 2025b; Stagakis, 2025a, 2025b, 2025c, 2025d; Stagakis, Chen, et al., 2025; Stagakis, Emberger, Buchmann, et al., 2025; Stagakis et al., 2025a, 2025b). Because no direct continuous measurements of the CO_2 exchange of whole trees and lawns were feasible, CO_2 fluxes were indirectly obtained by using the available measurements to constrain and calibrate a detailed, site-specific CO_2 exchange model representative for the trees and lawns in the respective parks (Stagakis, Bignotti, et al., 2025). The model is based on a canopy radiation transfer simulation using the observed LAI to estimate the radiation reaching the leaf surface across the vegetation canopy and a leaf-scale Farquhar model (Farquhar et al., 1980) for the estimation of leaf net photosynthesis and respiration. The

23284277, 2026, 3, Downloaded from https://agupubs.onlinelibrary.wiley.com/doi/10.1029/2025EF007458 by Dtsch Zentrum F. Luft-U. Raum Fahrt In D. Helmholtz Gemein., Wiley Online Library on [09/09/2026]. See the Terms and Conditions (https://onlinelibrary.wiley.com/terms-and-conditions) on Wiley Online Library for rules of use; OA articles are governed by the applicable Creative Commons License

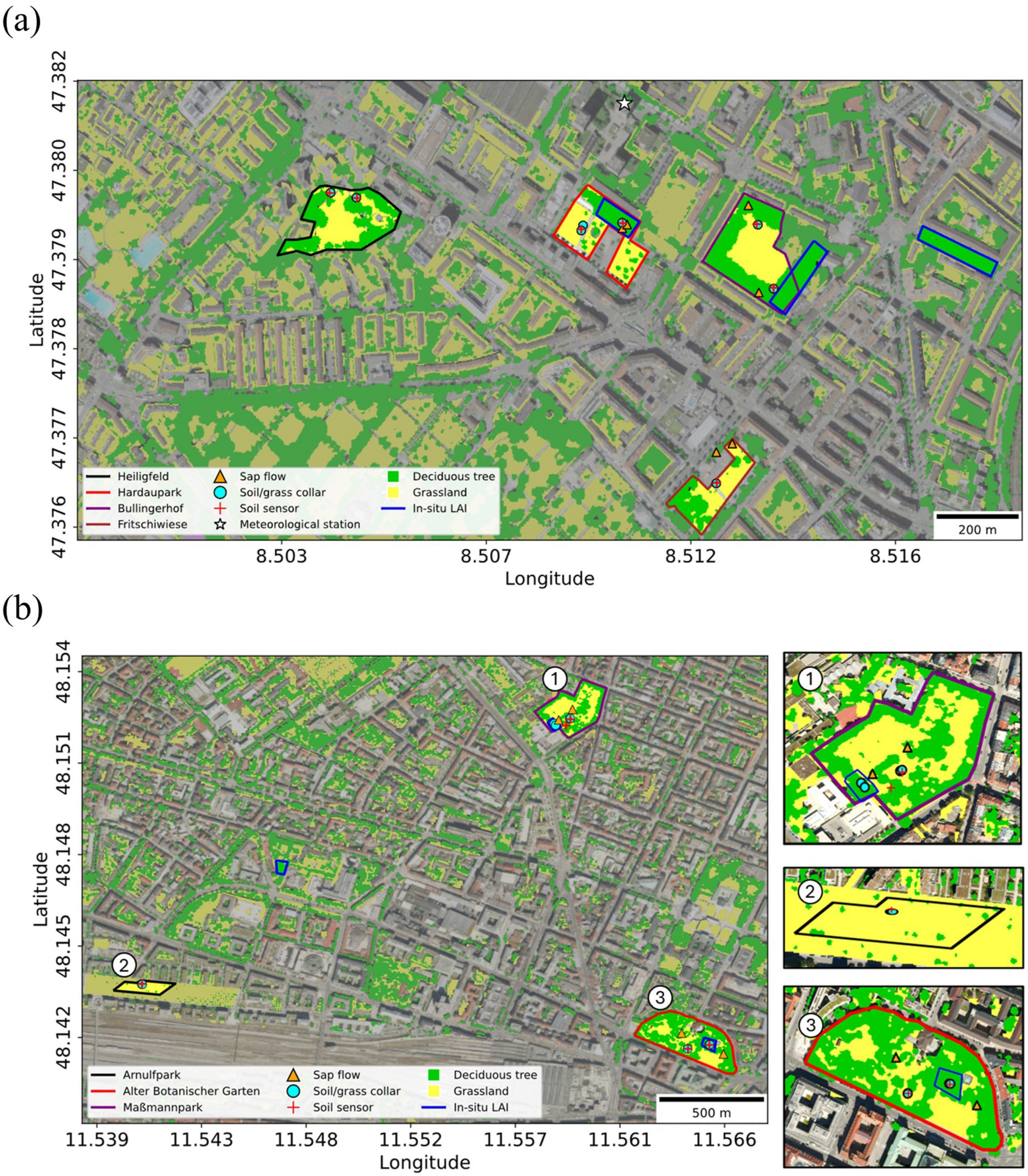

Figure 3. The location of vegetation and soil sensors, the boundaries of the study parks, and the vegetation land cover map at 1-m resolution, with background from satellite imagery in (a) Munich and (b) Zurich. Satellite image source: Esri, DigitalGlobe, GeoEye, i-cubed, USDA FSA, USGS, AEX, Getmapping, Aerogrid, IGN, IGP, swisstopo, and the GIS User Community (Esri, 2025).

23284277, 2026, 3, Downloaded from https://agupubs.onlinelibrary.wiley.com/doi/10.1029/2025EF007458 by Dtsch Zentrum F. Luft-U. Raum Fahrt In D. Helmholtz Gemein., Wiley Online Library on [09/09/2026]. See the Terms and Conditions (https://onlinelibrary.wiley.com/terms-and-conditions) on Wiley Online Library for rules of use; OA articles are governed by the applicable Creative Commons License

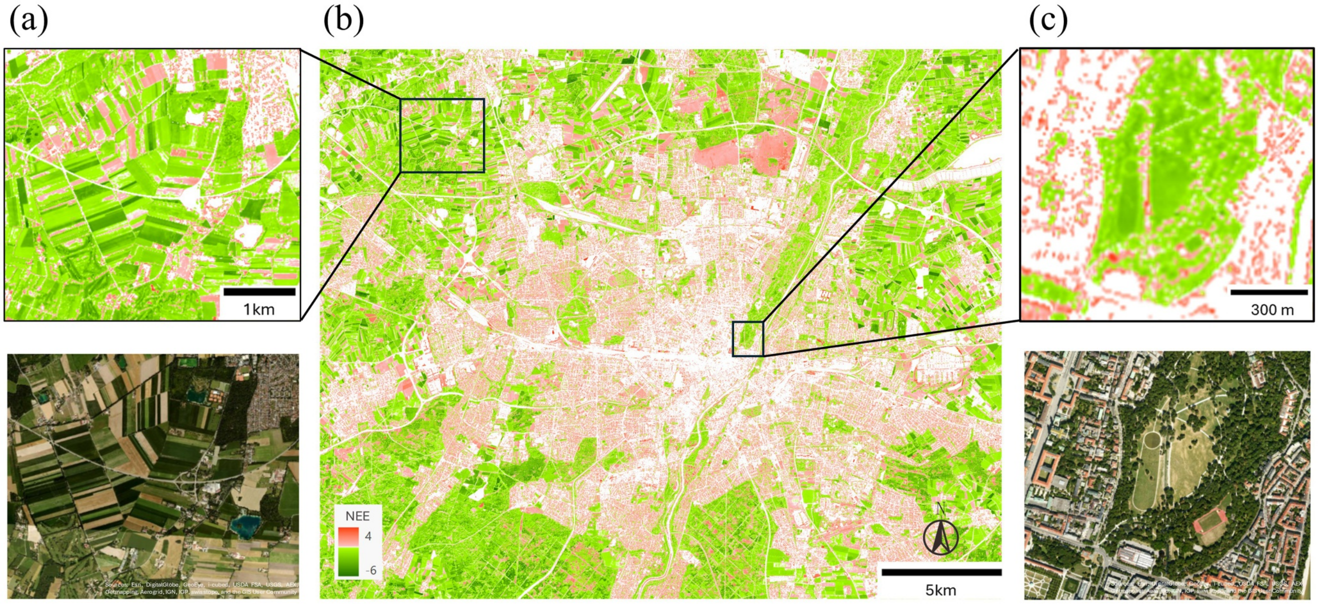

Figure 4. High-resolution biogenic CO_2 flux results for Munich in 2019 using standard VPRM. (a) Annual mean NEE results in an area dominated by cropland and the satellite image in the same location. (b) The annual mean CO_2 NEE map of Munich in 2019 using VPRM. (c) Annual mean NEE results at the south end of a large city park (English Garden) in Munich, as well as the corresponding satellite image in the same location. Satellite image source: Esri, DigitalGlobe, GeoEye, i-cubed, USDA FSA, USGS, AEX, Getmapping, Aerogrid, IGN, IGP, swisstopo, and the GIS User Community (Esri, 2025).

method is different for trees and lawns, as described in detail in the Supporting Information S1. In brief, tree sap flow observations were used to estimate hourly transpiration and stomatal conductance of the tree canopy, which was used to constrain the CO_2 supply in the Farquhar model. For lawns, stomatal conductance constraints on photosynthesis were simulated based on observations of the atmospheric vapor pressure deficit and ϑ. Soil respiration was modeled separately, applying the same approach for trees and lawns, using site-specific calibrations of a modified Lloyd and Taylor (1994) equation based on the T_{soil}, ϑ and chamber soil respiration measurements. A scientific publication providing a more detailed description is currently in preparation.

To facilitate the comparison, for each park, the VPRM results from trees within a 20 m radius surrounding each sap flow sensor were extracted and then averaged. Similarly, the VPRM results from the grassland in each park were averaged to represent the grassland simulation outcomes for each respective park.

3. Results

3.1. High-Resolution Biogenic Flux Estimation From Standard VPRM

3.1.1. Annual Biogenic CO_2 Flux

Figure 4 presents the annual mean CO_2 NEE map for Munich in 2019, derived using the standard VPRM model. A close examination of Figures 4a and 4c reveals that VPRM, when using high-resolution Sentinel-2, the vegetation land cover data we developed, and the simulated meteorological fields as inputs, can resolve differences in biogenic activity within the same or between different vegetation types, for example, between different cropland fields and small patches of grassland and trees in a forested city park. The total annual biogenic CO_2 flux estimated using the standard VPRM for 2019 was −167 kilotonnes of CO_2, while the UrbanVPRM and VPRM-modified versions yielded −236 kilotonnes CO_2 and −193 kilotonnes CO_2, respectively (see Table S6 in Supporting Information S1 for GEE and RE details). This represents approximately 2.0%–2.8% of Munich's anthropogenic emissions within the same area as shown in Figure 4b (8,341 kilotonnes of CO_2) (Tarakji & Gniffke, 2023).

Expanding on these spatial analyses, Figure 5 highlights the contributions of different vegetation types to the total NEE. Evergreen trees, despite covering the smallest amount of land (Figure 5a), absorbed the most CO_2, driven by their year-round photosynthesis (Figure 5b, Figure S4 in Supporting Information S1), while deciduous trees have

23284277, 2026, 3, Downloaded from https://agupubs.onlinelibrary.wiley.com/doi/10.1029/2025EF007458 by Dtsch Zentrum F. Luft-U. Raum Fahrt In D. Helmholtz Gemein., Wiley Online Library on [09/03/2026]. See the Terms and Conditions (https://onlinelibrary.wiley.com/terms-and-conditions) on Wiley Online Library for rules of use; OA articles are governed by the applicable Creative Commons License

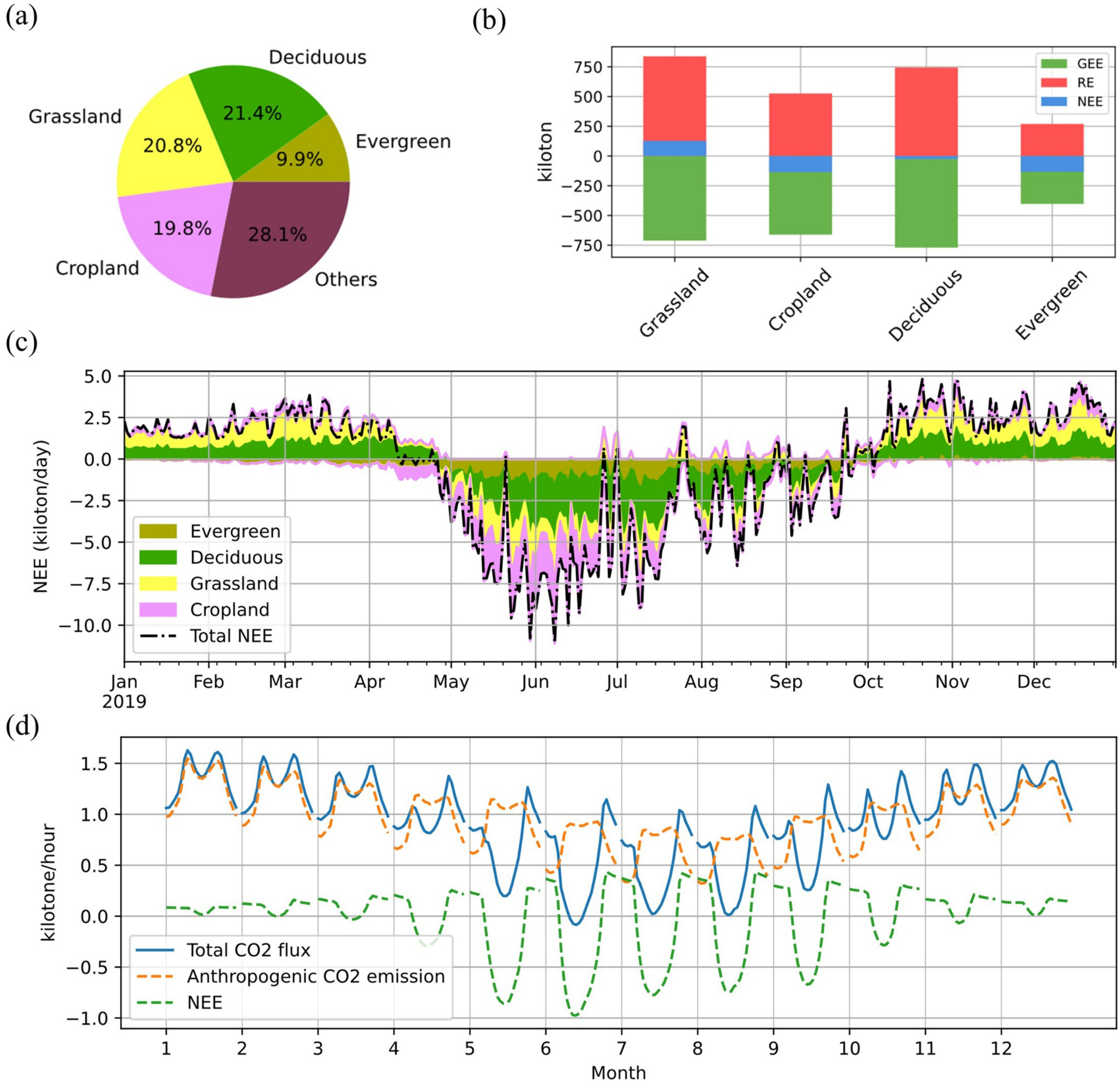

Figure 5. Contribution of different vegetation types to the total NEE and the comparison between anthropogenic CO_2 emission and NEE within the Munich study area. (a) The coverage of each vegetation type. (b) The annual total CO_2 flux of NEE, GEE, and Respiration. (c) Daily NEE contribution. (d) Comparison of the monthly diurnal cycle between anthropogenic CO_2 emission and NEE in Munich.

a low annual total CO_2 absorption (Figure 5b), largely attributed to their relatively high winter respiration (Figure 5c, Figure S4 in Supporting Information S1), and weak GEE from street trees, which were assumed to be deciduous. In contrast, grasslands act as a carbon source in Munich due to their high respiration (Figure 5c, Figure S4 in Supporting Information S1).

The monthly mean diurnal cycle of NEE can be compared to that of anthropogenic emissions (Tarakji & Gniffke, 2023) (Figure 5d). In warm seasons, CO_2 absorption by vegetation in Munich can match or even exceed anthropogenic emissions during the daytime, while during the winter months, the vegetation generally exhibited minimal CO_2 uptake, primarily driven by respiration from grasslands and deciduous trees.

23284277, 2026, 3, Downloaded from https://agupubs.onlinelibrary.wiley.com/doi/10.1029/2025EF007458 by Dtsch Zentrum F. Luft-U. Raum Fahrt In D. Helmholtz Gemein., Wiley Online Library on [09/09/2026]. See the Terms and Conditions (https://onlinelibrary.wiley.com/terms-and-conditions) on Wiley Online Library for rules of use; OA articles are governed by the applicable Creative Commons License

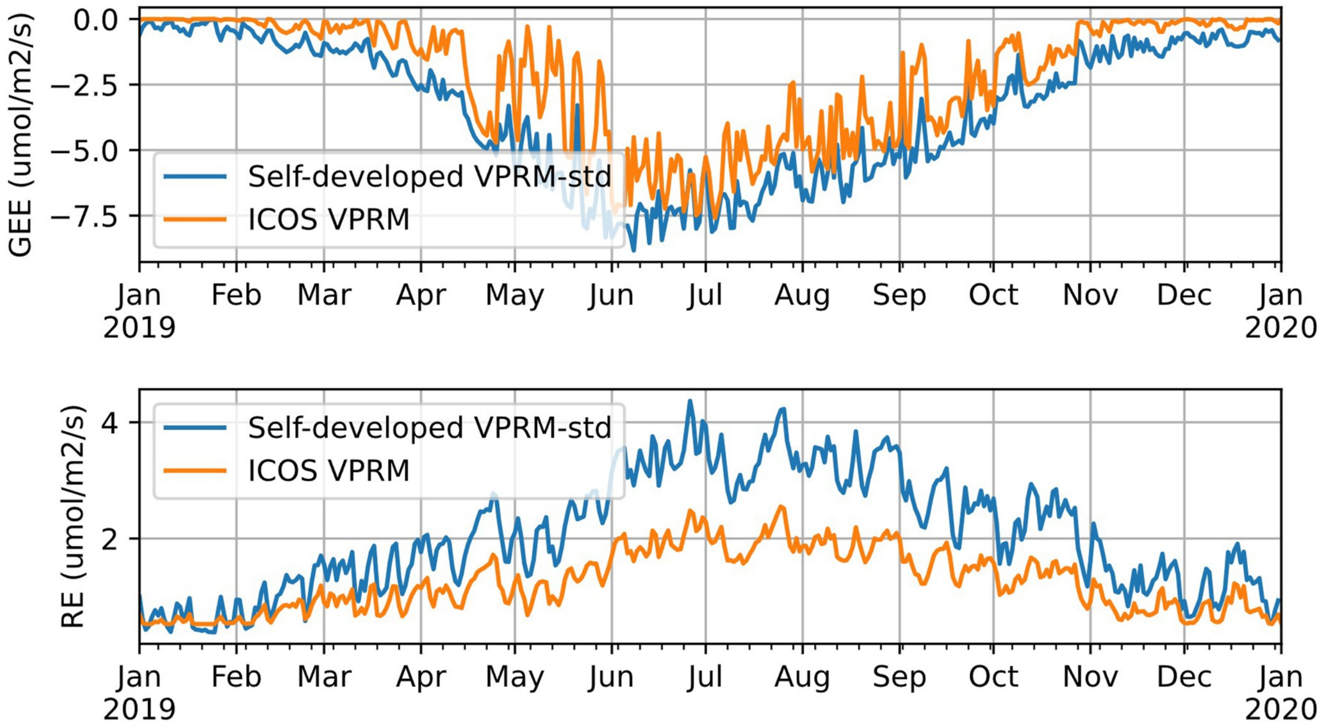

Figure 6. Daily mean VPRM results comparison between self-developed VPRM-std and ICOS-VPRM in Munich. The results are averaged across all extracted pixels.

3.1.2. Comparison of Self-Developed VPRM-Std With ICOS-VPRM Product

As illustrated in Figure 6, when applied to a larger domain encompassing substantially more vegetation and both driven by simulated meteorological results, our VPRM results based on standard VPRM (self-developed VPRM-std) exhibit higher GEE and significantly higher respiration on average while maintaining similar temporal behavior to ICOS-VPRM.

Figure 7 shows that in most rural areas, both models produce comparable results, with discrepancies primarily due to higher respiration in our VPRM, especially during winter. Within the Munich urban area (Figure 7b), the ICOS-VPRM reports nearly zero NEE throughout the year, whereas our VPRM effectively reproduces vegetation behaviors.

These differences arise largely from the contrasting land cover data sets and satellite-based vegetation indices. As can be seen in Figure S5 of Supporting Information S1, SYNMAP has only around 5% vegetation coverage in central Munich, while the landcover map we produced indicates approximately 46%. Additionally, the higher resolution of Sentinel-2 (10 m) compared to MODIS (500 m) also enhances the ability of our VPRM to simulate vegetation behaviors.

3.2. Comparison Between the Three Different Versions of VPRM

3.2.1. Comparison With Eddy Covariance Tower Observations in Different Ecosystems

As described in Section 2.3.2, we evaluated the performance of all three VPRM models using the NEE observation from ICOS ecosystem stations located in rural areas across Europe, with meteorological inputs sourced from individual station measurements. Note that for the UrbanVPRM, the respiration changes were applied only to trees, in line with the original paper (Hardiman et al., 2017a). Since all stations are in rural areas, the impervious surface areas are zero and the reference EVI is the same as the EVI of the pixel where the station is located. Consequently, UrbanVPRM is identical with the standard VPRM in terms of respiration.

Figure 8 demonstrate that all three VPRM models align well with the NEE observations. VPRM-modified exhibits a distinct behavior, particularly for respiration (Figure 8b), showing greater accuracy for grasslands and

23284277, 2026, 3, Downloaded from https://agupubs.onlinelibrary.wiley.com/doi/10.1029/2025EF007458 by Dtsch Zentrum F. Luft-U. Raum Fahrt In D. Helmholtz Gemein., Wiley Online Library on [09/03/2026]. See the Terms and Conditions (https://onlinelibrary.wiley.com/terms-and-conditions) on Wiley Online Library for rules of use; OA articles are governed by the applicable Creative Commons License

10.1029/2025EF007458

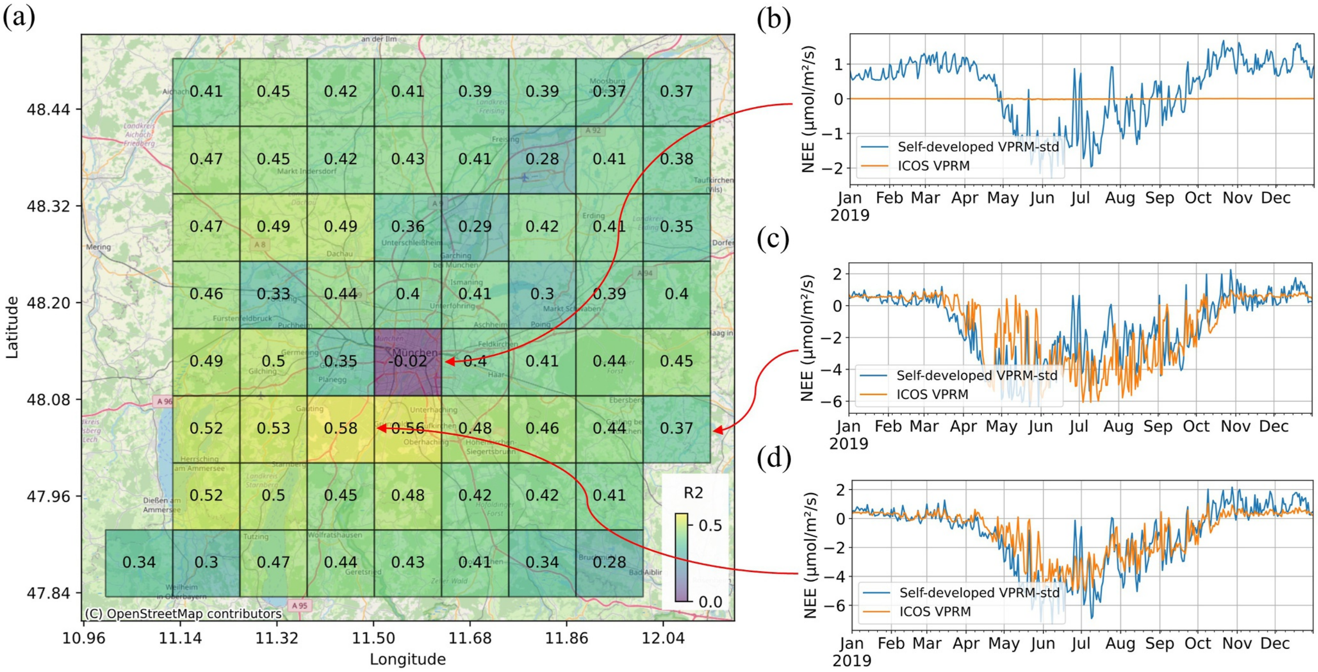

Figure 7. Comparison between self-developed VPRM-std and ICOS-VPRM in extracted ICOS-VPRM pixels. (a) Hourly R^2 (coefficient of determination) score map. The color and number in each pixel represent the R^2 score in these pixels. (b–d) Daily mean NEE comparison of selected pixels, the red arrows point to the corresponding pixels.

especially croplands compared to the other versions. Further analysis in Figure 9 and Figure S6 of Supporting Information S1 reveals that each model exhibits seasonal and diurnal errors in GEE, like an early onset growing season for deciduous trees, which critically determines the overall NEE accuracy. At the same time, UrbanVPRM's use of a different P_{scale}, using the EVI instead of LSWI (see Equations Y7 and Y5 in Supporting Information S1), showing a tiny increase in seasonal deviation compared with other VPRM models.

The VPRM-modified model more accurately replicates vegetation respiration during warmer seasons than other models, especially in capturing the seasonal dynamics of croplands. This enhanced performance is primarily due to integrating vegetation indices and incorporating non-linear temperature effects into its respiration formula.

3.2.2. Comparison With Urban Park Measurements

Due to the different environments in urban and suburban areas, comparing our results solely with observations in natural ecosystems is insufficient for assessing the effectiveness of the VPRM models in urban contexts. We also

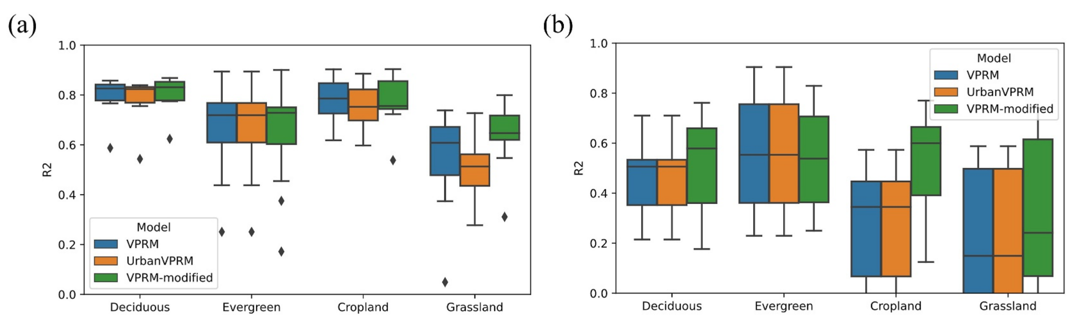

Figure 8. Boxplots of R^2 scores of the comparison between CO_2 fluxes measured at all selected eddy covariance towers with different VPRM models. For each site, only the hourly mean NEE data from the 2 years with the highest number of observations were selected. (a) Compared with all selected NEE data. (b) Compared with only the nighttime NEE in the selected observation data, which can be treated as ecosystem respiration due to the lack of photosynthesis at night.

23284277, 2026, 3, Downloaded from https://agupubs.onlinelibrary.wiley.com/doi/10.1029/2025EF007458 by Dtsch Zentrum F. Luft-U. Raum Fahrt In D. Helmholtz Gemein., Wiley Online Library on [09/09/2026]. See the Terms and Conditions (https://onlinelibrary.wiley.com/terms-and-conditions) on Wiley Online Library for rules of use; OA articles are governed by the applicable Creative Commons License

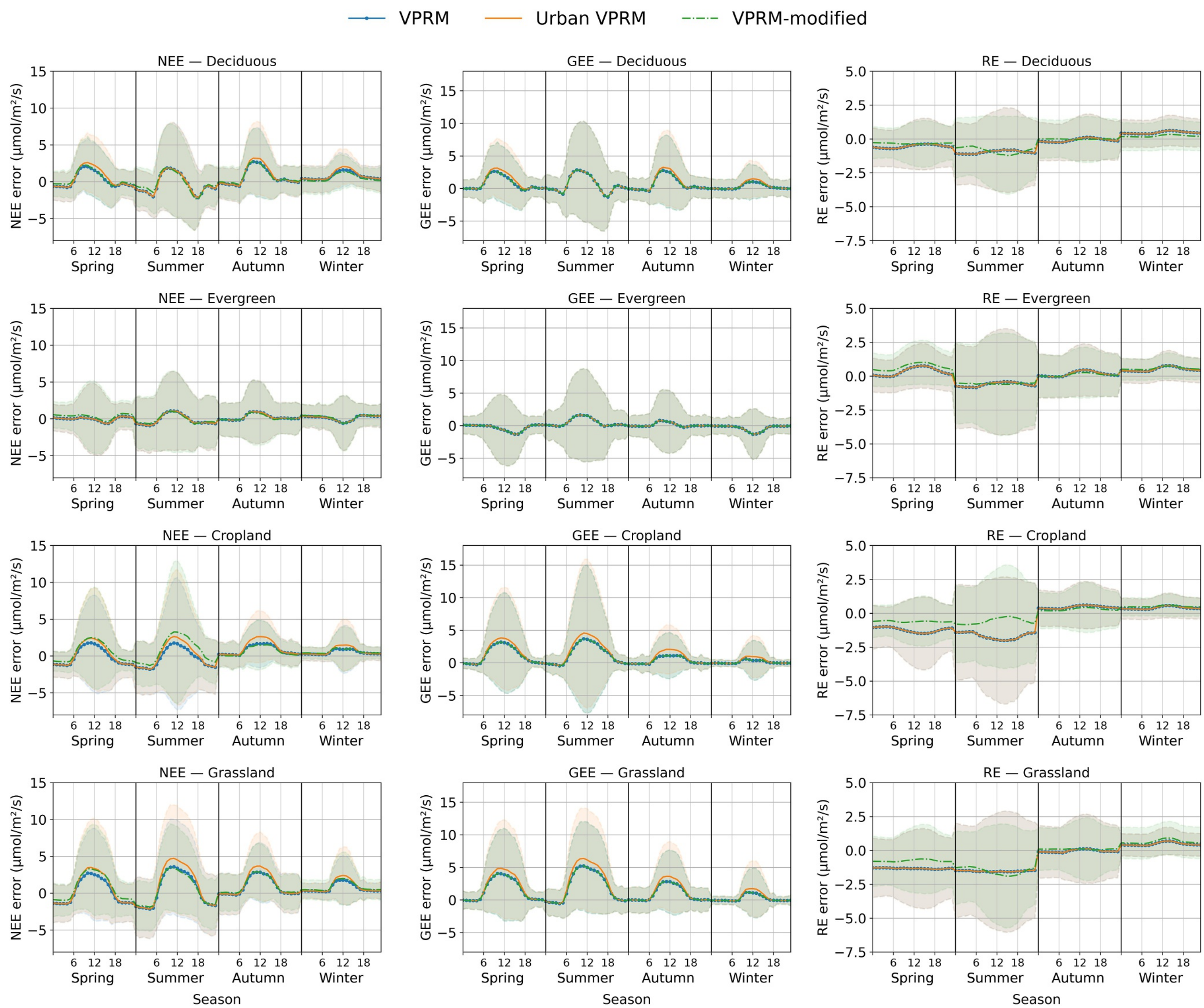

Figure 9. Diurnal cycle of each season for the error between VPRM models and observations across all selected eddy covariance towers. that is, Error = model results − observation. The opaque curves represent the mean of all errors in this type of data on the day of the year, while the semi-transparent dotted line and shaded area represent the corresponding ± standard deviation area. Seasons are defined as: Spring (Mar, Apr, May), Summer (Jun, Jul, Aug), Autumn (Sep, Oct, Nov), and Winter (Dec, Jan, Feb).

compared our VPRM results (driven by local station-observed meteorology) with observational outcomes from field measurements in selected urban parks in Munich and Zurich, as described in Section 2.3.3.

3.2.2.1. *Urban Trees*

We first compared the VPRMs' results with observations for urban deciduous trees, as illustrated in Figure 10 and Table 1. All VPRM models performed well in terms of GEE, although a too early onset of the growing season was observed (Figures 10b and 10e). The overall temporal evolution of respiration is also very well captured, but the models underestimate the summer respiration and overestimate the winter respiration (Figures 10c and 10f). The VPRM models thus take up too much CO_2 in summer and release too much CO_2 in winter in the parks. Due to the relatively lower EVI compared to the EVI_{ref} and the impervious surface area beneath some of the trees, the UrbanVPRM has the lowest respiration and accordingly the largest underestimation in summer (Figures 10c and 10f).

23284277, 2026, 3, Downloaded from https://agupubs.onlinelibrary.wiley.com/doi/10.1029/2025EF007458 by Dtsch Zentrum F. Luft-U. Raum Fahrt In D. Helmholtz Gemein, Wiley Online Library on [09/09/2026]. See the Terms and Conditions (https://onlinelibrary.wiley.com/terms-and-conditions) on Wiley Online Library for rules of use; OA articles are governed by the applicable Creative Commons License

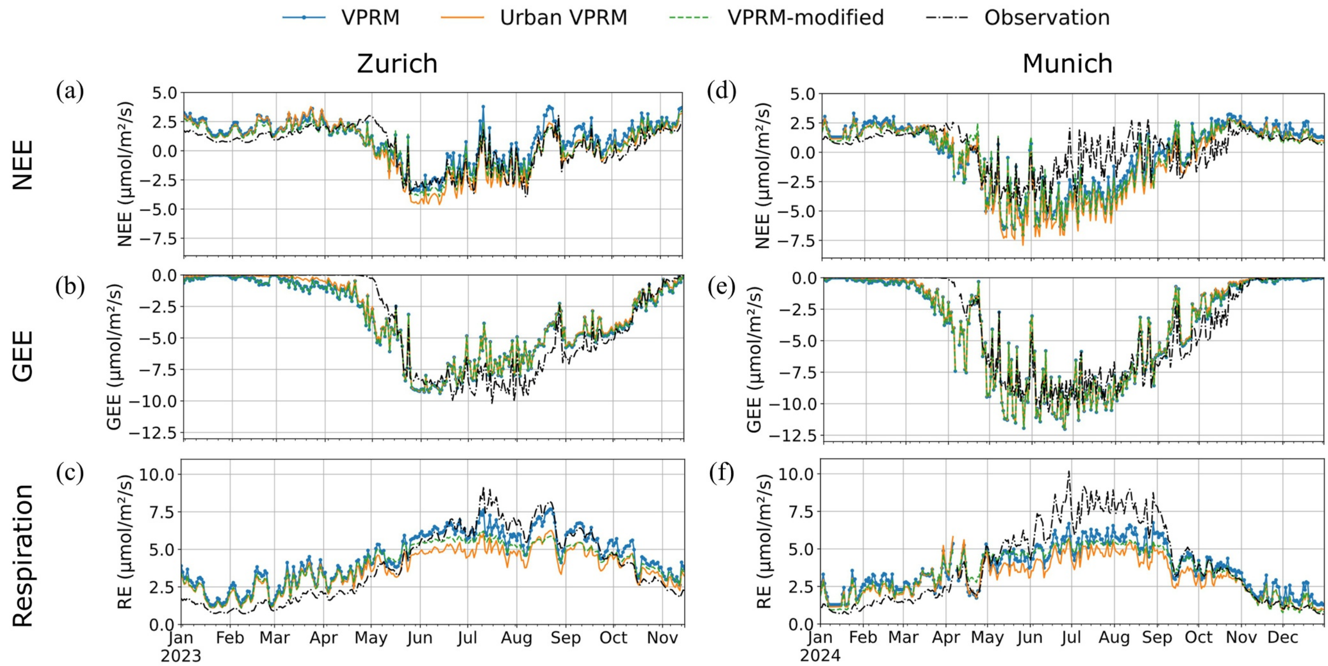

Figure 10. Daily mean comparison between each VPRM and field measurement in Munich and Zurich for trees averaged across all parks.

In the Fritschiwiese park in Zurich, as shown in Figure S7 of Supporting Information S1, the measured trees are surrounded by sealed surfaces (describe in Section 2.3.3). This landscape configuration results in lower pixel-averaged vegetation indices measured by Sentinel-2 and leads to lower GEE and, for VPRM-modified, also to reduced respiration.

3.2.2.2. Urban Park Lawns

The results of the VPRM models for lawns were compared with observational data from various parks. As presented in Figures 11a, 11b, 11d and 11e, as well as Table 2 and Table S5 in Supporting Information S1, the NEEs and GEEs estimated by each VPRM model exhibit a high correlation with the observed values ($R \approx 0.9$), indicating that the VPRM models can effectively capture these biogenic carbon flux dynamics.

The respiration from lawns estimated by the VPRM models was generally overestimated in winter periods (Figures 11c and 11f). The VPRM-modified model exhibited improved seasonal performance, better capturing the respiration variability of Zurich's urban lawns and the elevated summer respiration in Munich's urban lawns. This discrepancy between the observations and both VPRM and UrbanVPRM models suggests that the linear relationship inadequately represents the connection between respiration and temperature.

Table 1
Performance of the VPRM Models Simulated Hourly NEE in μmol/m²/s Compared With In Situ Observation-Based Carbon Fluxes From Trees in Zurich and Munich City Parks

Park	UrbanVPRM			VPRM			VPRM-modified		
Model	*R*	*R*2	RMSE (μmol/m²/s)	*R*	*R*2	RMSE (μmol/m²/s)	*R*	*R*2	RMSE (μmol/m²/s)
Bullingerhof (Zurich)	0.94	0.87	1.94	0.94	0.87	1.94	0.94	0.89	1.83
Fritschiwiese (Zurich)	0.91	0.82	2.04	0.9	0.82	2.54	0.91	0.82	2.05
Hardau (Zurich)	0.95	0.88	1.76	0.95	0.88	1.7	0.95	0.88	1.73
Alter Botanischer Garten (Munich)	0.83	0.53	3.5	0.84	0.57	3.32	0.83	0.54	3.46
Maßmannpark (Munich)	0.82	0.64	3.32	0.83	0.68	3.12	0.83	0.66	3.22

Note. The performance for GEE and respiration separately is shown in Table S4 of Supporting Information S1.

23284277, 2026, 3, Downloaded from https://agupubs.onlinelibrary.wiley.com/doi/10.1029/2025EF007458 by Dtsch Zentrum F. Luft-U. Raum Fahrt In D. Helmholtz Gemein., Wiley Online Library on [09/09/2026]. See the Terms and Conditions (https://onlinelibrary.wiley.com/terms-and-conditions) on Wiley Online Library for rules of use; OA articles are governed by the applicable Creative Commons License

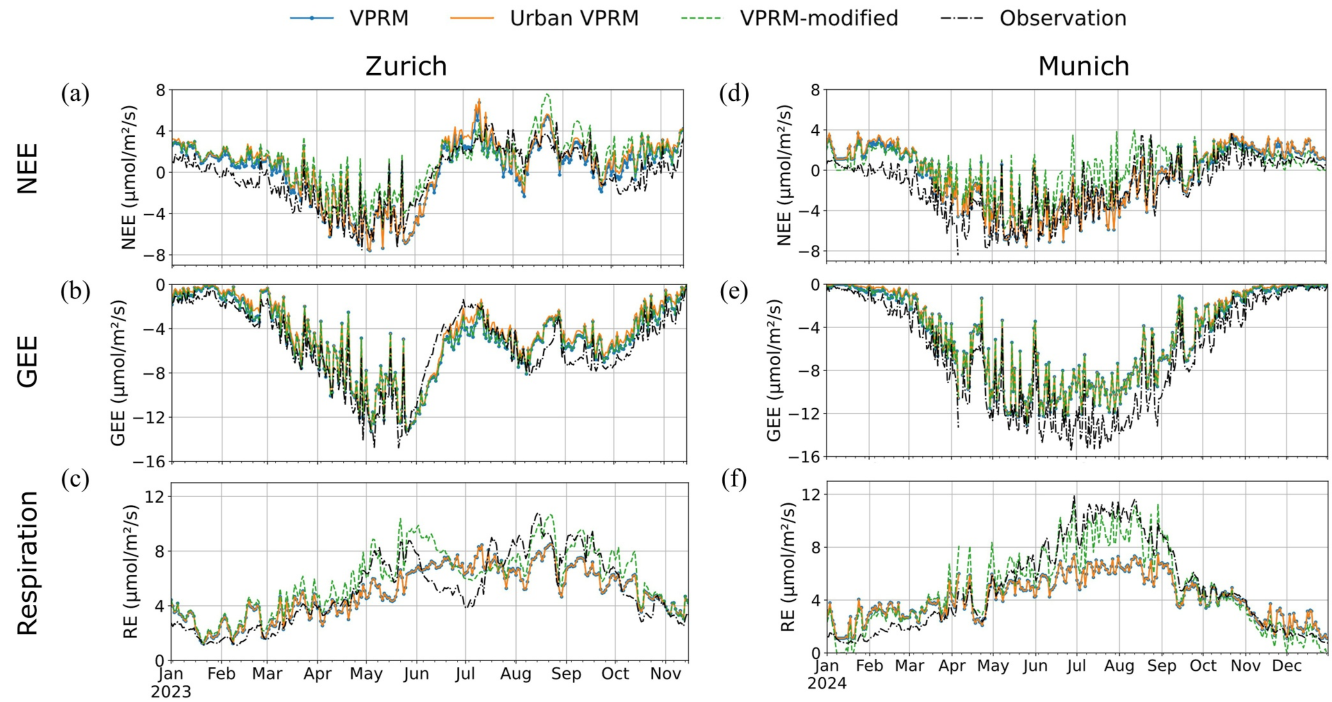

Figure 11. Daily mean comparison between each VPRMs results and field measurement results in Munich and Zurich for grassland averaged across all parks.

3.2.3. Comparison Between VPRMs' Simulation Results

The VPRM, UrbanVPRM, and VPRM-modified models were deployed in the study domains in both Munich and Zurich, driven by simulated meteorological fields in both cities. The annual mean NEE map of all three models can be found in Figure 4, Figures S8 and S9 of Supporting Information S1, while the annual total NEE, GEE and ecosystem respiration estimated by the three models are shown in Table S6 of Supporting Information S1.

In all three VPRM models, trees show higher CO_2 uptake than other vegetation types (Figure 12). Both the UrbanVPRM and VPRM-modified models exhibit lower ecosystem respiration for trees compared to the VPRM (Figure 13), and therefore, estimate more negative net CO_2 fluxes (i.e., stronger net uptake) as shown in Figure S10a of Supporting Information S1. For deciduous trees, UrbanVPRM has a slightly weaker photosynthesis uptake in winter and the lowest respiration due to impervious surfaces below street trees, leading to the highest net CO_2 uptake.

Table 2
Performance of the VPRM Models Simulated NEE in μmol/m²/s Compared With In Situ Observation-Based Carbon Fluxes From Grassland in Zurich and Munich City Parks

Park	UrbanVPRM			VPRM			VPRM-modified		
Model	R	*R2*	RMSE (μmol/m²/s)	*R*	*R2*	RMSE (μmol/m²/s)	*R*	*R2*	RMSE (μmol/m²/s)
Bulingerhof (Zurich)	0.93	0.85	3.03	0.94	0.88	2.66	0.95	0.84	3.1
Fritschiwiese (Zurich)	0.89	0.78	3.49	0.9	0.81	3.24	0.9	0.79	3.43
Hardau (Zurich)	0.94	0.86	2.77	0.95	0.9	2.37	0.95	0.87	2.66
Arnulfpark (Munich)	0.89	0.76	4.4	0.89	0.77	4.3	0.89	0.72	4.68
Alter Botanischer Garten (Munich)	0.87	0.72	4.43	0.88	0.74	4.31	0.86	0.67	4.8
Maßmannpark (Munich)	0.88	0.73	4.54	0.89	0.75	4.38	0.87	0.68	4.98

Note. The separate comparisons for GEE and respiration are shown in Table S5 of Supporting Information S1.

23284277, 2026, 3, Downloaded from https://agupubs.onlinelibrary.wiley.com/doi/10.1029/2025EF007458 by Dtsch Zentrum F. Luft-U. Raum Fahrt In D. Helmholtz Gemein., Wiley Online Library on [09/09/2026]. See the Terms and Conditions (https://onlinelibrary.wiley.com/terms-and-conditions) on Wiley Online Library for rules of use; OA articles are governed by the applicable Creative Commons License

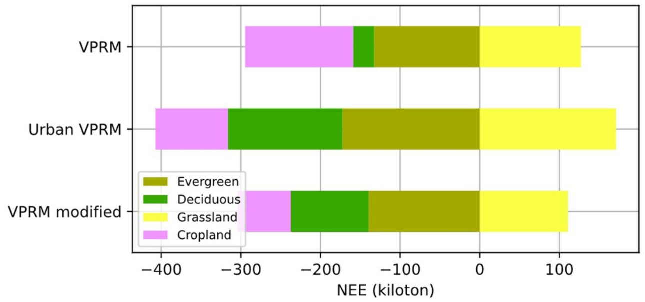

Figure 12. Contributions of different vegetation types to annual mean NEE in different VPRM models in Munich.

For croplands (see Figure 13), the VPRM-modified and UrbanVPRM models estimate lower CO_2 absorption, due to the higher ecosystem respiration and lower GEE, respectively. Grasslands consistently act as net CO_2 sources across all models (Figure 12). Through the integration of the high resolution vegetation indices in the respiration formula, the VPRM-modified model demonstrated enhanced seasonal variations and revealed different behaviors among managed and unmanaged grasslands (Figures S10c and S10d in Supporting Information S1) and between different croplands (Figure S10b in Supporting Information S1).

Figure S12a in Supporting Information S1 reveals that 35.2% of vegetation areas include impervious surfaces, mainly near deciduous trees and grasslands. As shown in Figure S12b of Supporting Information S1, ISA-containing mixed pixels have a substantial impact on NEE estimation, consistent with our comparison to Fritschiwiese park observations in Zurich (Section 3.2.2).

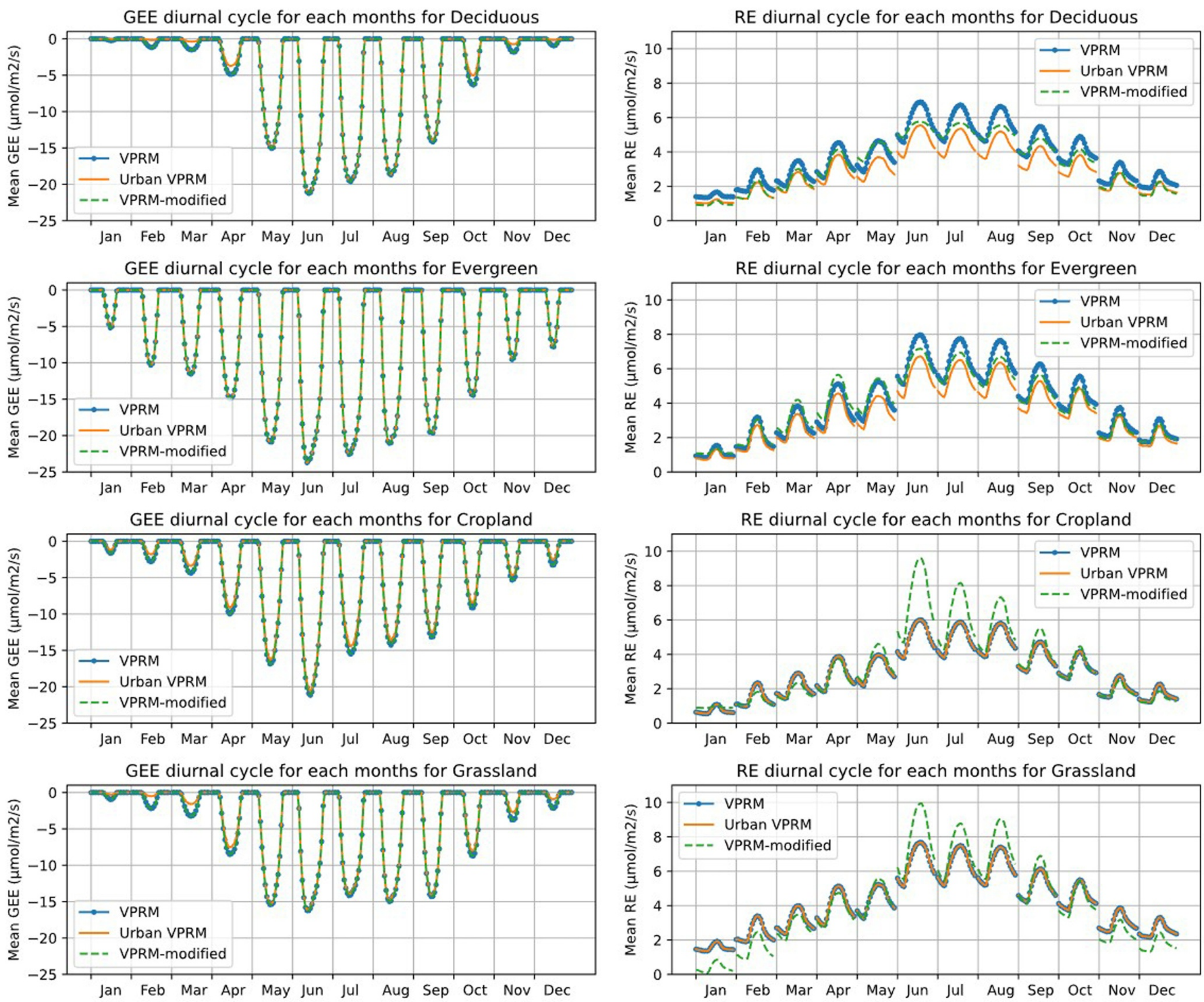

Figure 13. Comparison of each month's diurnal cycle of GEE and RE of different vegetation types by each VPRM model. The comparison NEE results are present in Figure S11 of Supporting Information S1.

23284277, 2026, 3, Downloaded from https://agupubs.onlinelibrary.wiley.com/doi/10.1029/2025EF007458 by Dtsch Zentrum F. Luft-U. Raum Fahrt In D. Helmholtz Gemein, Wiley Online Library on [09/09/2026]. See the Terms and Conditions (https://onlinelibrary.wiley.com/terms-and-conditions) on Wiley Online Library for rules of use; OA articles are governed by the applicable Creative Commons License

23284277, 2026, 3, Downloaded from https://agupubs.onlinelibrary.wiley.com/doi/10.1029/2025EF007458 by Dtsch Zentrum F. Luft-U. Raum Fahrt In D. Helmholtz Gemein., Wiley Online Library on [09/03/2026]. See the Terms and Conditions (https://onlinelibrary.wiley.com/terms-and-conditions) on Wiley Online Library for rules of use; OA articles are governed by the applicable Creative Commons License

4. Discussion

This study presents a high-resolution framework to estimate urban biogenic CO_2 fluxes using the VPRM model, which effectively enhances the accuracy and spatial detail of biogenic CO_2 flux estimations in complex urban landscapes. Given the distinct photosynthetic and respiratory behaviors of different types of vegetation, utilizing land cover maps at high spatial resolution is essential (Coleman et al., 2020; Parazoo et al., 2022). Our self-developed high-resolution land cover maps precisely capture fragmented urban green spaces, such as street trees, small lawns, and city parks, that are missing in coarse-resolution maps (Figure S3 in Supporting Information S1), as well as in moderate-resolution global land cover products derived from Landsat and MODIS (Huang et al., 2021; Ju et al., 2022). Even in suburban areas, forests are comprised of diverse tree species and are interspersed with grasslands and built-up areas, leading to variable NEE behavior (Su et al., 2021; Čepelová & Münzbergová, 2012). Similarly, large continuous croplands or grasslands display spatial and temporal heterogeneity due to factors like harvest frequency and fallow periods, respectively. Fine-grained vegetation indices derived from Sentinel-2 imagery are thus critical for accurately capturing these dynamic patterns (Tiruneh et al., 2023). Due to the combination of high-resolution land cover and Sentinel-2 derived indices, our VPRM models can effectively capture vegetation carbon flux inside urban areas. The great benefits of our high-resolution framework are particularly notable when compared with results from lower-resolution VPRM products.

Based on our high-resolution VPRM results for Munich, we estimate an annual total biogenic CO_2 NEE is −167 kilotons for 2019 within the study area using the standard VPRM (−236 kilotons for UrbanVPRM and −193 kilotons for VPRM-modified), accounting for approximately 2.0%–2.8% of the region's total anthropogenic emissions. This finding is consistent with values reported for other cities, such as ∼2% in Boston (Hardiman et al., 2017b) and ∼7% in Helsinki (Havu et al., 2024). Note that our study area focuses primarily on the city itself, with most forests and croplands located beyond its boundaries; thus, expanding the domain would likely alter this proportion. In 2019, from June to August, the modeled daytime uptake of CO_2 in our VPRM urban domain occasionally matched or even exceeded anthropogenic emissions, highlighting the important carbon-buffering potential of urban vegetation. Similar patterns have been reported for Boston (Sargent et al., 2018) and Toronto (Madsen-Colford et al., 2025). Previous studies in cities such as Winbourne et al. (2022), Baltimore (Hill et al., 2021), and others (Wang et al., 2022) have shown that forests generally absorb more carbon than grasslands, though grasslands may act as intermittent carbon sinks or sources. Our findings in Munich clarify that for our study area, trees act as the dominant contributors to CO_2 uptake, while, in contrast, grasslands exhibited positive annual NEE values, indicating that they are net carbon sources. Our high-resolution VPRM results also reveal that the flux among various types of grasslands differ significantly, and even adjacent croplands can exhibit different NEE characteristics.

This variability can likely be attributed to disparities in phenological stages, influenced by factors such as crop species, management practices, and cultivation cycles (Gottschalk et al., 2024; Zhang et al., 2020). These findings underscore the unique advantage of high-resolution remote sensing in accurately detecting adjacent vegetation cover and ecologically distinct green space types, enhancing the precision of urban biogenic carbon flux estimates.

This study further compared three versions of the VPRM to evaluate their adaptability to urban environments. All models aligned well with eddy covariance observations in rural areas across Europe and showed strong temporal correlations with NEE observations at urban deciduous trees and lawns in Munich and Zurich parks. However, they revealed limitations in reproducing growing season onset GEE—potentially stemming from the inability of reflectance-based vegetation indices to accurately represent seasonal dynamics (Walther et al., 2016; Zhang et al., 2022)—as well as in the magnitude of respiration in the parks. Compared to the original, the VPRM-modified model, incorporating a nonlinear temperature-respiration relation, better captured seasonal variations in suburban croplands and grasslands. The UrbanVPRM model, with its EVI-ISA correction, aims to improve urban flux estimates, particularly by reducing respiration estimates for street trees (Figures S10a and S12b in Supporting Information S1).

Current model parameters, primarily derived from rural area observations, fail to account for distinct urban vegetation phenological and physiological characteristics, including variations in soil moisture, biomass, and human interventions such as irrigation and fertilization (Stagakis, Brunner, et al., 2025) or litter removal (Li et al., 2024; Totzki et al., 2025). The deviations observed in our respiration estimates for urban parks highlight limitations in model adaptability to urban contexts. Moreover, mixed pixels containing both vegetation and

23284277, 2026, 3, Downloaded from https://agupubs.onlinelibrary.wiley.com/doi/10.1029/2025EF007458 by Dtsch Zentrum F. Luft-U. Raum Fahrt In D. Helmholtz Gemein., Wiley Online Library on [09/03/2026]. See the Terms and Conditions (https://onlinelibrary.wiley.com/terms-and-conditions) on Wiley Online Library for rules of use; OA articles are governed by the applicable Creative Commons License

impervious surfaces—accounting for approximately 35% of vegetated pixels in Munich (Figure S12a in Supporting Information S1)—introduce additional uncertainty into urban carbon flux estimations. As demonstrated in Figure S13 of Supporting Information S1 and consistent with findings in multiple studies (Li et al., 2023; Yuan & Bauer, 2007), this ISA contamination systematically reduces vegetation indices, leading to underestimation of biogenic net CO_2 uptake. In Section 3.2.2, the underprediction of GEE for street trees in Zurich's Fritschiwiese Park reinforces the sensitivity of flux estimates to pixel purity. While UrbanVPRM accounts for these tree understory impacts, its validation is hindered by the limited urban observations and the suburban origin of the parameter sets. Thus, future research should focus on extensive observations of diverse urban green spaces and the development of urban-specific parameter sets to enhance model applicability. Furthermore, evaluating the spatial transferability of these parameters will be equally crucial to determine whether city-specific sets are generalizable to regions with similar bioclimatic conditions, or whether high vegetation heterogeneity necessitates localized calibrations to ensure model robustness.

Conflict of Interest

The authors declare no conflicts of interest relevant to this study.

Data Availability Statement

The code for all models and the results necessary for this manuscript are available at Zenodo via https://doi.org/10.5281/zenodo.18318382. The "Sentinel-2 MSI—Level 2A (MAJA Tiles)—Germany" data set was produced by the German Aerospace Center (DLR) (German Aerospace Center, 2019). The following data sets for Munich were obtained from the Bavarian State Office for Digitisation, High-Speed Internet and Surveying (LDBV) (Geobasisdaten: Bayerische Vermessungsverwaltung—www.geodaten.bayern.de (Data modified), Licensed under CC BY 4.0.): the Real Estate Cadastre Information System (ALKIS) land use map, laser point cloud data, and the building coverage data set. The Imperviousness Density 2018, Urban Atlas, Street Tree Layer, and CLC + Backbone data sets were sourced from the Copernicus Land Monitoring Service (European Environment Agency, 2020a, 2020c). The ESA World Cover map data set is attributed to Zanaga et al. (2022).

Acknowledgments
This research has been supported by the European Union's Horizon 2020 programme (Grant 101037319) in the framework of the ICOS Cities project (Pilot Applications in Urban Landscapes (PAUL)—Towards integrated city observatories for greenhouse gases), the European Research Council (ERC) Consolidator Grant CoSense4Climate (Grant 101089203, PI: Jia Chen), the China Scholarship Council (Grant 202108330044), and the ICOS Switzerland (ICOS-CH) Phase 4 (Swiss National Science Foundation, Grant 20FI-0_229655) is also acknowledged. We also thank Dr. Stephen Starck from the Language Center at the Technical University of Munich for his valuable assistance with the language of the manuscript. Additionally, the ChatGPT-4o language model developed by OpenAI was also used to improve the manuscript's language. Open Access funding enabled and organized by Projekt DEAL.

References

Ahmadov, R., Gerbig, C., Kretschmer, R., Körner, S., Rödenbeck, C., Bousquet, P., & Ramonet, M. (2009). Comparing high resolution WRF-VPRM simulations and two global CO_2 transport models with coastal tower measurements of CO_2. *Biogeosciences*, *6*(5), 807–817. https://doi.org/10.5194/bg-6-807-2009

Askar, Nuthammachot, N., Phairuang, W., Wicaksono, P., & Sayektiningsih, T. (2018). Estimating aboveground biomass on private forest using Sentinel-2 imagery. *Journal of Sensors, 2018*, 1–11. https://doi.org/10.1155/2018/6745629

Baldocchi, D., Falge, E., Gu, L., Olson, R., Hollinger, D., Running, S., et al. (2001). FLUXNET: A new tool to study the temporal and spatial variability of ecosystem–scale carbon dioxide, water vapor, and energy flux densities. *Bulletin of the American Meteorological Society*, *82*(11), 2415–2434. https://doi.org/10.1175/1520-0477(2001)082<2415:fantts>2.3.co;2

Bayerische Vermessungsverwaltung. (2024). Geobasisdaten [Geobase data] [Dataset]. Retrieved from https://www.geodaten.bayern.de

Bezyk, Y., Sówka, I., & Górka, M. (2021). Assessment of urban CO_2 budget: Anthropogenic and biogenic inputs. *Urban Climate*, *39*, 100949. https://doi.org/10.1016/j.uclim.2021.100949

Čepelová, B., & Münzbergová, Z. (2012). Factors determining the plant species diversity and species composition in a suburban landscape. *Landscape and Urban Planning*, *106*(4), 336–346. https://doi.org/10.1016/j.landurbplan.2012.04.008

Chen, F., Yang, X., & Zhu, W. (2014). WRF simulations of urban heat island under hot-weather synoptic conditions: The case study of Hangzhou City, China. *Atmospheric Research*, *138*, 364–377. https://doi.org/10.1016/j.atmosres.2013.12.005

Cleveland, W. S. (1979). Robust locally weighted regression and smoothing scatterplots. *Journal of the American Statistical Association*, *74*(368), 829–836. https://doi.org/10.1080/01621459.1979.10481038

Coleman, R. W., Stavros, N., Yadav, V., & Parazoo, N. (2020). A simplified framework for high-resolution urban vegetation classification with optical imagery in the Los Angeles megacity. *Remote Sensing*, *12*(15), 2399. https://doi.org/10.3390/rs12152399

Esri. (2024). ArcGIS pro (version 3.1). *Esri*. Retrieved from https://www.esri.com/en-us/arcgis/products/arcgis-pro/overview

Esri. (2025). *World imagery [basemap]. Scale not given*. World Imagery Map. Retrieved from https://www.arcgis.com/home/item.html?id=10df2279f9684e4a9f6a7f08febac2a9

European Environment Agency. (2020). *Imperviousness density 2018 (raster 10 m), Europe, 3-yearly, Aug. 2020 (version 01.00) [GeoTIFF]*. European Environment Agency. https://doi.org/10.2909/3BF542BD-EEBD-4D73-B53C-A0243F2ED862

European Environment Agency. (2020). *Urban Atlas land cover/land use 2018 (vector), Europe, 6-yearly, Jul. 2021 (version 01.03) [Geopackage]*. European Environment Agency. https://doi.org/10.2909/FB4DFFA1-6CEB-4CC0-8372-1ED354C285E6

European Space Agency. (2022). Sentinel-2 MSI Level-2A BOA reflectance [Dataset]. https://doi.org/10.5270/S2_-znk9xsj

European Environment Agency. (2019). *CORINE land cover 2018 (raster 100 m), Europe, 6-yearly—Version 2020_20u1, May 2020 (version 20.01) [GeoTIFF]*. European Environment Agency. https://doi.org/10.2909/960998C1-1870-4E82-8051-6485205EBBAC

European Environment Agency. (2020c). *Urban Atlas street tree layer 2018 (vector), Europe, 6-yearly, Feb. 2021 (version 01.02) [Geopackage]*. European Environment Agency. https://doi.org/10.2909/205691B3-7AE9-41DD-ABF1-1FBF60D72C8C

European Environment Agency. (2024). *CLC+Backbone 2021 (raster 10 m), Europe, 3-yearly, Jun. 2024 (version 01.00) [GeoTIFF]*. European Environment Agency. https://doi.org/10.2909/71FC9D1B-479F-4DA1-AA66-662A2FFF2CF7

Farquhar, G. D., Von Caemmerer, S., & Berry, J. A. (1980). A biochemical model of photosynthetic CO_2 assimilation in leaves of C_3 species. *Planta*, *149*(1), 78–90. https://doi.org/10.1007/BF00386231

Gerbig, C., & Koch, F.-T. (2023). Biosphere-atmosphere exchange fluxes for CO_2 from the vegetation photosynthesis and respiration model VPRM for 2006–2022 (version 1.1). [NetCDF files]. *ICOS-ERIC—Carbon Portal*. https://doi.org/10.18160/VX78-HVA1

German Aerospace Center. (2019). Sentinel-2 MSI—Level 2A (MAJA tiles)—Germany [Dataset]. *German Aerospace Center (DLR)*. https://doi.org/10.15489/IFCZSSZKCP63

German Aerospace Center (DLR). (2025). Terrabyte: An operational platform for remote sensing data analysis. Retrieved from https://www.dlr.de/en/eoc/research-transfer/projects-missions/terrabyte

Giorgetta, M. A., Jungclaus, J., Reick, C. H., Legutke, S., Bader, J., Böttinger, M., et al. (2013). Climate and carbon cycle changes from 1850 to 2100 in MPI-ESM simulations for the coupled model intercomparison project phase 5. *Journal of Advances in Modeling Earth Systems*, *5*(3), 572–597. https://doi.org/10.1002/jame.20038

Glauch, T., Marshall, J., Gerbig, C., Botía, S., Gałkowski, M., Vardag, S. N., & Butz, A. (2025). pyVPRM: A next-generation vegetation photosynthesis and respiration model for the post-MODIS era. *Geoscientific Model Development*, *18*(14), 4713–4742. https://doi.org/10.5194/gmd-18-4713-2025

Gottschalk, P., Kalhori, A., Li, Z., Wille, C., & Sachs, T. (2024). Monitoring cropland daily carbon dioxide exchange at field scales with Sentinel-2 satellite imagery. *Biogeosciences*, *21*(16), 3593–3616. https://doi.org/10.5194/bg-21-3593-2024

Gourdji, S. M., Karion, A., Lopez-Coto, I., Ghosh, S., Mueller, K. L., Zhou, Y., et al. (2022). A modified vegetation photosynthesis and respiration model (VPRM) for the Eastern USA and Canada, evaluated with comparison to atmospheric observations and other biospheric models. *Journal of Geophysical Research*, *127*, e2021JG006290. https://doi.org/10.1029/2021JG006290

Hardiman, B. S., Wang, J. A., Hutyra, L. R., Gately, C. K., Getson, J. M., & Friedl, M. A. (2017). Accounting for urban biogenic fluxes in regional carbon budgets. *Science of the Total Environment*, *592*, 366–372. https://doi.org/10.1016/j.scitotenv.2017.03.028

Havu, M., Kulmala, L., Lee, H. S., Saranko, O., Soininen, J., Ahongshangbam, J., & Järvi, L. (2024). CO_2 uptake of urban vegetation in a warming Nordic city. *Urban Forestry and Urban Greening*, *94*, 128261. https://doi.org/10.1016/j.ufug.2024.128261

Hersbach, H., Bell, B., Berrisford, P., Hirahara, S., Horányi, A., Muñoz-Sabater, J., et al. (2020). The ERA5 global reanalysis. *Quarterly Journal of the Royal Meteorological Society*, *146*(730), 1999–2049. https://doi.org/10.1002/qj.3803

Hill, A. C., Barba, J., Hom, J., & Vargas, R. (2021). Patterns and drivers of multi-annual CO_2 emissions within a temperate suburban neighborhood. *Biogeochemistry*, *152*(1), 35–50. https://doi.org/10.1007/s10533-020-00731-1

Huang, C., Yang, J., Clinton, N., Yu, L., Huang, H., Dronova, I., & Jin, J. (2021). Mapping the maximum extents of urban green spaces in 1039 cities using dense satellite images. *Environmental Research Letters*, *16*(6), 064072. https://doi.org/10.1088/1748-9326/ac03dc

Huete, A., Didan, K., Miura, T., Rodriguez, E. P., Gao, X., & Ferreira, L. G. (2002). Overview of the radiometric and biophysical performance of the MODIS vegetation indices. *Remote Sensing of Environment*, *83*(1–2), 195–213. https://doi.org/10.1016/S0034-4257(02)00096-2

ICOS, R. I., Aalto, J., Aalto, P., Aaltonen, H., Aiguier, T., Akubia, J., et al. (2024). *Ecosystem final quality (L2) product in ETC-archive format—Release 2024-1 (version 1.0) [Arbitrary ZIP archive, ICOS ETC half-hourly product CSV]*. ICOS ERIC—Carbon Portal. https://doi.org/10.18160/G5KZ-ZD83

Järvi, L., Grimmond, C. S. B., & Christen, A. (2011). The surface urban energy and water balance scheme (SUEWS): Evaluation in Los Angeles and Vancouver. *Journal of Hydrology*, *411*(3–4), 219–237. https://doi.org/10.1016/j.jhydrol.2011.10.001

Järvi, L., Havu, M., Ward, H. C., Bellucco, V., McFadden, J. P., Toivonen, T., et al. (2019). Spatial modeling of local-scale biogenic and anthropogenic carbon dioxide emissions in Helsinki. *Journal of Geophysical Research: Atmospheres*, *124*(15), 8363–8384. https://doi.org/10.1029/2018JD029576

Järvi, L., Rannik, Ü., Kokkonen, T. V., Kurppa, M., Karppinen, A., Kouznetsov, R. D., et al. (2018). Uncertainty of eddy covariance flux measurements over an urban area based on two towers. *Atmospheric Measurement Techniques*, *11*(10), 5421–5438. https://doi.org/10.5194/amt-11-5421-2018

Ju, Y., Dronova, I., & Delclòs-Alió, X. (2022). A 10 m resolution urban green space map for major Latin American cities from Sentinel-2 remote sensing images and OpenStreetMap. *Scientific Data*, *9*(1), 586. https://doi.org/10.1038/s41597-022-01701-y

Jung, M., Henkel, K., Herold, M., & Churkina, G. (2006). Exploiting synergies of global land cover products for carbon cycle modeling. *Remote Sensing of Environment*, *101*(4), 534–553. https://doi.org/10.1016/j.rse.2006.01.020

Lan, C., Mauder, M., & Mauder, M. (2025). *Biogenic in-situ observations (L2), Munich PAR, 2023-03-23–2024-12-31 (version 1.0) [Generic CSV]*. ICOS ERIC - Carbon Portal. https://doi.org/10.18160/N7D3-EW9F

LAStools. (2003). Efficient LiDAR processing software (version 230731). Retrieved from http://rapidlasso.com/LAStools

Li, H., Zhou, Y., Wang, X., Zhou, X., Zhang, H., & Sodoudi, S. (2019). Quantifying urban heat island intensity and its physical mechanism using WRF/UCM. *Science of the Total Environment*, *650*, 3110–3119. https://doi.org/10.1016/j.scitotenv.2018.10.025

Li, J., Chen, J., & Chen, J. (2025a). *Biogenic in situ observations (L2), Munich LAI, 2024-04-08–2024-08-14 (version 1.0) [Generic CSV]*. ICOS ERIC - Carbon Portal. https://doi.org/10.18160/6ARV-14R6

Li, J., Chen, J., & Chen, J. (2025b). *Biogenic in situ observations (L2), Munich Soil respiration, 2024-03-26–2024-11-27 (version 1.0) [Generic CSV]*. ICOS ERIC - Carbon Portal. https://doi.org/10.18160/XJAR-DNRX

Li, P., Wang, Z.-H., & Wang, C. (2024). The potential of urban irrigation for counteracting carbon-climate feedback. *Nature Communications*, *15*(1), 2437. https://doi.org/10.1038/s41467-024-46826-3

Li, S., Zhou, Z., Ma, R., Liu, S., & Guan, Q. (2023). Extracting subpixel vegetation NDVI time series for evaluating the mixed pixel effect on GPP estimation in urban areas. *International Journal of Digital Earth*, *16*(1), 3222–3238. https://doi.org/10.1080/17538947.2023.2246945

Lloyd, J., & Taylor, J. A. (1994). On the temperature dependence of soil respiration. *Functional Ecology*, *8*(3), 315. https://doi.org/10.2307/2389824

Madsen-Colford, S., Hutyra, L., Smith, I., Wu, D., Arain, M. A., Staebler, R., et al. (2025). Modification and comparison of two urban vegetation models over Southern Ontario, Canada. *Journal of Geophysical Research: Biogeosciences*, *130*(9), e2025JG008943. https://doi.org/10.1029/2025JG008943

Mahadevan, P., Wofsy, S. C., Matross, D. M., Xiao, X., Dunn, A. L., Lin, J. C., et al. (2008). A satellite-based biosphere parameterization for net ecosystem CO_2 exchange: Vegetation photosynthesis and respiration model (VPRM). *Global Biogeochemical Cycles*, *22*(2), 2006GB002735. https://doi.org/10.1029/2006GB002735

Menzer, O., & McFadden, J. P. (2017). Statistical partitioning of a three-year time series of direct urban net CO_2 flux measurements into biogenic and anthropogenic components. *Atmospheric Environment*, *170*, 319–333. https://doi.org/10.1016/j.atmosenv.2017.09.049

Meyer, L., Brinkman, S., van Kesteren, L., Leprince-Ringuet, N., & van Boxmeer, F. (2014). Technical support unit for the synthesis report.

23284277, 2026, 3, Downloaded from https://agupubs.onlinelibrary.wiley.com/doi/10.1029/2025EF007458 by Dtsch Zentrum F. Luft-U. Raum Fahrt In D. Helmholtz Gemein., Wiley Online Library on [09/09/2026]. See the Terms and Conditions (https://onlinelibrary.wiley.com/terms-and-conditions) on Wiley Online Library for rules of use; OA articles are governed by the applicable Creative Commons License

23284277, 2026, 3, Downloaded from https://agupubs.onlinelibrary.wiley.com/doi/10.1029/2025EF007458 by Dtsch Zentrum F. Luft-U. Raum Fahrt In D. Helmholtz Gemein., Wiley Online Library on [09/03/2026]. See the Terms and Conditions (https://onlinelibrary.wiley.com/terms-and-conditions) on Wiley Online Library for rules of use; OA articles are governed by the applicable Creative Commons License

Parazoo, N. C., Coleman, R. W., Yadav, V., Stavros, E. N., Hulley, G., & Hutyra, L. (2022). Diverse biosphere influence on carbon and heat in mixed urban Mediterranean landscape revealed by high resolution thermal and optical remote sensing. *Science of the Total Environment*, *806*, 151335. https://doi.org/10.1016/j.scitotenv.2021.151335

Ponomarev, N., Steiner, M., Koene, E., Constantin, L., Rubli, P., Emmenegger, L., & Brunner, D. (2023). Application of the ICON-ART model for CO_2 fluxes estimation in the city of Zurich. https://doi.org/10.5194/egusphere-egu23-7542

Reick, C. H., Raddatz, T., Brovkin, V., & Gayler, V. (2013). Representation of natural and anthropogenic land cover change in MPI-ESM. *Journal of Advances in Modeling Earth Systems*, *5*(3), 459–482. https://doi.org/10.1002/jame.20022

Rosentreter, J. A. (2022). Water-air gas exchange of CO_2 and CH_4 in coastal wetlands. In *Carbon mineralization in coastal wetlands* (pp. 167–196). Elsevier. https://doi.org/10.1016/B978-0-12-819220-7.00003-0

Sargent, M., Barrera, Y., Nehrkorn, T., Hutyra, L. R., Gately, C. K., Jones, T., et al. (2018). Anthropogenic and biogenic CO_2 fluxes in the Boston urban region. *Proceedings of the National Academy of Sciences*, *115*(29), 7491–7496. https://doi.org/10.1073/pnas.1803715115

Schimel, D. S. (1995). Terrestrial ecosystems and the carbon cycle. *Global Change Biology*, *1*(1), 77–91. https://doi.org/10.1111/j.1365-2486.1995.tb00008.x

Seto, K. C., Dhakal, S., Bigio, A., Blanco, H., Delgado, G. C., Dewar, D., et al. (2014). Human settlements, infrastructure, and spatial planning. *Human Settlements*.

Son, N.-T., Chen, C.-F., Chen, C.-R., & Guo, H.-Y. (2020). Classification of multitemporal Sentinel-2 data for field-level monitoring of rice cropping practices in Taiwan. *Advances in Space Research*, *65*(8), 1910–1921. https://doi.org/10.1016/j.asr.2020.01.028

Stagakis, S. (2025a). *Biogenic in situ observations (L2), Munich leaf photosynthesis, 2024-07-23–2024-07-25 (version 1.0) [Generic CSV]*. ICOS ERIC - Carbon Portal. https://doi.org/10.18160/J48H-14Y6

Stagakis, S. (2025b). *Biogenic in situ observations (L2), Zurich leaf photosynthesis, 2022-08-26–2023-08-18 (version 1.0) [Generic CSV]*. ICOS ERIC - Carbon Portal. https://doi.org/10.18160/VADT-Q6YV

Stagakis, S. (2025c). *Biogenic in situ observations (L2), Zurich PAR, 2022-07-12–2024-12-31 (version 1.0) [Generic CSV]*. ICOS ERIC - Carbon Portal. https://doi.org/10.18160/6VNY-JE78

Stagakis, S. (2025d). *Biogenic in situ observations (L2), Zurich soil sensors, 2022-05-15–2024-12-31 (version 1.0) [Generic CSV]*. ICOS ERIC - Carbon Portal. https://doi.org/10.18160/P6CM-9V1E

Stagakis, S., Bignotti, L., Li, J., Emberger, S., Loubet, B., Fortineau, A., et al. (2025). Assessing the biogenic CO_2 fluxes in urban green areas using an observation-constrained modelling approach. https://doi.org/10.5194/icuc12-407

Stagakis, S., Brunner, D., Li, J., Backman, L., Karvonen, A., Constantin, L., et al. (2025). Intercomparison of biogenic CO_2 flux models in four urban parks in the city of Zurich. *Biogeosciences*, *22*(9), 2133–2161. https://doi.org/10.5194/bg-22-2133-2025

Stagakis, S., Chen, J., Li, J., Chen, J., & Li, J. (2025). *Biogenic in-situ observations (L2), Munich sapflow, 2024-04-01–2024-12-31 (version 1.0) [Generic CSV]*. ICOS ERIC - Carbon Portal. https://doi.org/10.18160/SPBJ-67W7

Stagakis, S., Emberger, S., Buchmann, N., Emberger, S., & Buchmann, N. (2025). *Biogenic in-situ observations (L2), Zurich sapflow, 2022-06-30–2024-12-01 (version 1.0) [Generic CSV]*. ICOS ERIC - Carbon Portal. https://doi.org/10.18160/E7RK-YH5A

Stagakis, S., Emberger, S., & Emberger, S. (2025a). *Biogenic in-situ observations (L2), Zurich Soil respiration, 2022-07-27–2024-07-26 (version 1.0) [Generic CSV]*. ICOS ERIC - Carbon Portal. https://doi.org/10.18160/49K2-Y0WA

Stagakis, S., Emberger, S., & Emberger, S. (2025b). *Biogenic in-situ observations (L2), Zurich LAI, 2022-04-13–2023-10-06 (version 1.0) [Generic CSV]*. ICOS ERIC - Carbon Portal. https://doi.org/10.18160/Y7F0-5WJ6

Stagakis, S., Feigenwinter, C., Vogt, R., Brunner, D., & Kalberer, M. (2023). A high-resolution monitoring approach of urban CO_2 fluxes. Part 2 – Surface flux optimisation using eddy covariance observations. *Science of the Total Environment*, *903*, 166035. https://doi.org/10.1016/j.scitotenv.2023.166035

Stagakis, S., Feigenwinter, C., Vogt, R., & Kalberer, M. (2023). A high-resolution monitoring approach of urban CO_2 fluxes. Part 1—Bottom-up model development. *Science of the Total Environment*, *858*, 160216. https://doi.org/10.1016/j.scitotenv.2022.160216

Steiner, M., Peters, W., Luijkx, I., Henne, S., Chen, H., Hammer, S., & Brunner, D. (2024). European CH_4 inversions with ICON-ART coupled to the CarbonTracker data assimilation shell. *Atmospheric Chemistry and Physics*, *24*(4), 2759–2782. https://doi.org/10.5194/acp-24-2759-2024

Su, Y., Gong, C., Cui, B., Guo, P., Ouyang, Z., & Wang, X. (2021). Spatial heterogeneity of plant diversity within and between neighborhoods and its implications for a plant diversity survey in urban areas. *Forests*, *12*(4), 416. https://doi.org/10.3390/f12040416

Tarakji, Y., & Gniffke, P. (2023). National inventory report for the German greenhouse gas inventory 1990—2021.

Thölix, L., Backman, L., Havu, M., Karvinen, E., Soininen, J., Trémeau, J., et al. (2025). Carbon sequestration in different urban vegetation types in Southern Finland. *Biogeosciences*, *22*(3), 725–749. https://doi.org/10.5194/bg-22-725-2025

Tiruneh, G. A., Meshesha, D. T., Adgo, E., Tsunekawa, A., Haregeweyn, N., Fenta, A. A., et al. (2023). Mapping crop yield spatial variability using Sentinel-2 vegetation indices in Ethiopia. *Arabian Journal of Geosciences*, *16*(11), 631. https://doi.org/10.1007/s12517-023-11754-x

Totzki, J., Blumenstein, K., & Saha, S. (2025). Urban soil respiration patterns: An analysis of Quercus Robur vs. Quercus Rubra in parks and streets of Karlsruhe, Germany. *Urban Forestry and Urban Greening*, *107*, 128814. https://doi.org/10.1016/j.ufug.2025.128814

Turnbull, J. C., Karion, A., Davis, K. J., Lauvaux, T., Miles, N. L., Richardson, S. J., et al. (2019). Synthesis of urban CO_2 emission estimates from multiple methods from the Indianapolis flux project (INFLUX). *Environmental Science & Technology*, *53*(1), 287–295. https://doi.org/10.1021/acs.est.8b05552

Velasco, E., & Roth, M. (2010). Cities as net sources of CO_2: Review of atmospheric CO_2 exchange in urban environments measured by eddy covariance technique. *Geography Compass*, *4*(9), 1238–1259. https://doi.org/10.1111/j.1749-8198.2010.00384.x

Walther, S., Voigt, M., Thum, T., Gonsamo, A., Zhang, Y., Köhler, P., et al. (2016). Satellite chlorophyll fluorescence measurements reveal large-scale decoupling of photosynthesis and greenness dynamics in boreal evergreen forests. *Global Change Biology*, *22*(9), 2979–2996. https://doi.org/10.1111/gcb.13200

Wang, R., Mattox, C. M., Phillips, C. L., & Kowalewski, A. R. (2022). Carbon sequestration in turfgrass–soil systems. *Plants*, *11*(19), 2478. https://doi.org/10.3390/plants11192478

Wei, D., Reinmann, A., Schiferl, L. D., & Commane, R. (2022). High resolution modeling of vegetation reveals large summertime biogenic CO_2 fluxes in New York City. *Environmental Research Letters*, *17*(12), 124031. https://doi.org/10.1088/1748-9326/aca68f

Weissert, L. F., Salmond, J. A., & Schwendenmann, L. (2014). A review of the current progress in quantifying the potential of urban forests to mitigate urban CO_2 emissions. *Urban Climate*, *8*, 100–125. https://doi.org/10.1016/j.uclim.2014.01.002

Winbourne, J. B., Smith, I. A., Stoynova, H., Kohler, C., Gately, C. K., Logan, B. A., et al. (2022). Quantification of urban forest and Grassland carbon fluxes using field measurements and a satellite-based model in Washington DC/Baltimore area. *Journal of Geophysical Research: Biogeosciences*, *127*(1), e2021JG006568. https://doi.org/10.1029/2021JG006568

23284277, 2026, 3, Downloaded from https://agupubs.onlinelibrary.wiley.com/doi/10.1029/2025EF007458 by Dtsch Zentrum F. Luft-U. Raum Fahrt In D. Helmholtz Gemein., Wiley Online Library on [09/09/2026]. See the Terms and Conditions (https://onlinelibrary.wiley.com/terms-and-conditions) on Wiley Online Library for rules of use; OA articles are governed by the applicable Creative Commons License

Wu, D., Lin, J. C., Duarte, H. F., Yadav, V., Parazoo, N. C., Oda, T., & Kort, E. A. (2021). A model for urban biogenic CO_2 fluxes: Solar-induced fluorescence for modeling urban biogenic fluxes (SMUrF v1). *Geoscientific Model Development*, *14*(6), 3633–3661. https://doi.org/10.5194/gmd-14-3633-2021

Wu, K., Davis, K. J., Miles, N. L., Richardson, S. J., Lauvaux, T., Sarmiento, D. P., et al. (2022). Source decomposition of eddy-covariance CO_2 flux measurements for evaluating a high-resolution urban CO_2 emissions inventory. *Environmental Research Letters*, *17*(7), 074035. https://doi.org/10.1088/1748-9326/ac7c29

Yang, B., Zhang, Y., & Qian, Y. (2012). Simulation of urban climate with high-resolution WRF model: A case study in Nanjing, China. *Asia-Pacific Journal of Atmospheric Sciences*, *48*(3), 227–241. https://doi.org/10.1007/s13143-012-0023-5

Yuan, F., & Bauer, M. E. (2007). Comparison of impervious surface area and normalized difference vegetation index as indicators of surface urban heat island effects in Landsat imagery. *Remote Sensing of Environment*, *106*(3), 375–386. https://doi.org/10.1016/j.rse.2006.09.003

Zanaga, D., Van De Kerchove, R., Daems, D., De Keersmaecker, W., Brockmann, C., Kirches, G., et al. (2022). ESA WorldCover 10 m 2021 v200 (version v200) [Dataset]. *Zenodo*. https://doi.org/10.5281/ZENODO.7254221

Zhang, J., Xiao, J., Tong, X., Zhang, J., Meng, P., Li, J., et al. (2022). NIRv and SIF better estimate phenology than NDVI and EVI: Effects of spring and autumn phenology on ecosystem production of planted forests. *Agricultural and Forest Meteorology*, *315*, 108819. https://doi.org/10.1016/j.agrformet.2022.108819

Zhang, Q., Lei, H., Yang, D., Xiong, L., Liu, P., & Fang, B. (2020). Decadal variation in CO_2 fluxes and its budget in a wheat and maize rotation cropland over the North China plain. *Biogeosciences*, *17*(8), 2245–2262. https://doi.org/10.5194/bg-17-2245-2020

Zhao, X., Chen, J., Marshall, J., Gałkowski, M., Hachinger, S., Dietrich, F., et al. (2023). Understanding greenhouse gas (GHG) column concentrations in Munich using the weather research and forecasting (WRF) model. *Atmospheric Chemistry and Physics*, *23*(22), 14325–14347. https://doi.org/10.5194/acp-23-14325-2023

Zürich Kanton. (2025). Amtliche vermessung. Retrieved from https://www.zh.ch/de/planen-bauen/geoinformation/kataster/amtliche-vermessung.html

References From the Supporting Information

Campbell, G. S., & Norman, J. M. (1998). *An introduction to environmental biophysics*. Springer New York. https://doi.org/10.1007/978-1-4612-1626-1

Forster, M. A. (2019). The dual method approach (DMA) resolves measurement range limitations of heat pulse velocity sap flow sensors. *Forests*, *10*(1), 46. https://doi.org/10.3390/f10010046

Forster, M. A., Kim, T. D. H., Kunz, S., Abuseif, M., Chulliparambil, V. R., Srichandra, J., & Michael, R. N. (2022). Phenology and canopy conductance limit the accuracy of 20 evapotranspiration models in predicting transpiration. *Agricultural and Forest Meteorology*, *315*, 108824. https://doi.org/10.1016/j.agrformet.2022.108824

Gebauer, T., Horna, V., & Leuschner, C. (2008). Variability in radial sap flux density patterns and sapwood area among seven co-occurring temperate broad-leaved tree species. *Tree Physiology*, *28*(12), 1821–1830. https://doi.org/10.1093/treephys/28.12.1821